examined the expression profiles of *Dicer* and *eIF2C1~4* during the myogenic differentiation of C2C12 cells and compared them with those of skeletal muscle examined above. As shown in Fig. 3, the expression profiles reveal that the level of expression of either *Dicer* or *eIF2C1~3* is gradually decreased during the myogenic differentiation of C2C12 cells, and that the *eIF2C4* gene is expressed at a low level in either C2C12 myoblast or myotube.

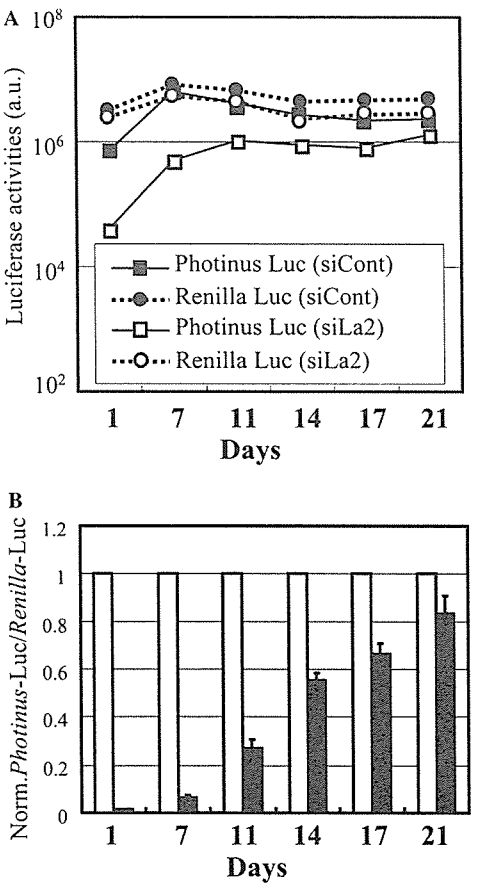

Fig. 4. Persistence of RNAi activity during myogenic differentiation of mouse C2C12 cells. The La2 siRNA duplex or a non-silencing siRNA duplex (Qiagen) together with pGL3-control and pRL-SV40 plasmids were cotransfected into C2C12 cells as in Fig. 2. Before transfection, the culture medium (DMEM containing 15% fetal calf serum) was replaced with DMEM containing 5% horse serum for induction of the myogenic differentiation of C2C12 cells. RNAi activity was examined 24 h after transfection (day 1), and thereafter examined at various days (indicated) up to 3 weeks after the transfection. (A) Absolute *Photinus* and *Renilla* luciferase expressions. The expression levels are plotted in arbitrary luminescence units (a.u.). (B) Ratios of normalised target to control luciferase. Ratios of normalised target (*Photinus*) luciferase activity to control (*Renilla*) luciferase activity are indicated as in Fig. 2. Open and solid bars indicate the data in the presence of the non-silencing siRNA and La2 siRNA duplexes, respectively. Data are averages of at least three independent experiments. Error bars represent standard deviations.

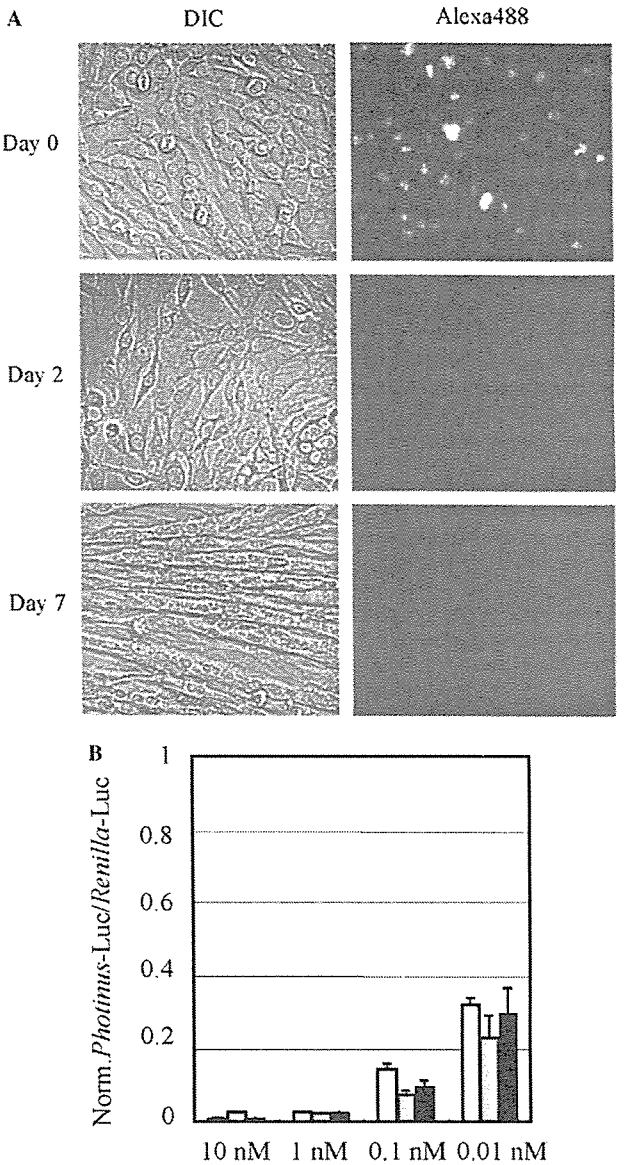

Fig. 5. Cell-cycle arrest and RNAi activity during myogenic differentiation of C2C12 cells. Myogenic differentiation of C2C12 cells was induced by changing the culture medium from DMEM containing 15% fetal calf serum to DMEM containing 5% horse serum. (A) Cell-cycle arrested C2C12 cells. Metabolically labeling of the cells with BrdU was carried out at indicated days after the differentiation. Day 0 indicates undifferentiated C2C12 cells. BrdU incorporated into the cells was visualised with an anti-BrdU antibody and an Alexa488 conjugated secondary antibody. The cells were examined by a florescent microscope. Left (DIC, differential interference contrast) and right (Alexa488, florescence image) panels are identical in visual field. (B) RNAi activity during the differentiation. The reporter plasmids carrying the *Photinus* and *Renilla luciferase* genes were cotransfected with a decreasing amount of the La2 siRNA or non-silencing siRNA duplexes (Qiagen), from 10 to 0.01 nM, into either undifferentiated or differentiated C2C12 cells. Ratios of normalised target (*Photinus*) luciferase activity to control (*Renilla*) luciferase activity are indicated as in Fig. 2. Open, dotted, and solid bars indicate the data in C2C12 cells that differentiated for 0 (undifferentiated), 2, and 7 days, respectively. Data are averages of at least three independent experiments. Error bars represent standard deviations.

Next we examined RNAi activity during the myogenic differentiation of C2C12 cells. The La2 siRNA duplex together with pGL3-control and pRL-SV40 plasmids was cotransfected into undifferentiated C2C12 cells, and simultaneously myogenic differentiation of the cells was carried out by changing culture medium as described above (see Materials and methods). As a result, a strong RNAi activity was detected by day 7 after RNAi induction (Fig. 4), when morphological changes of C2C12 cells into myotubes appeared to be completed (Fig. 5A); thereafter, the cells gradually lost the RNAi activity and lost most of the activity by day 21 after the induction (Fig. 4).

Because proliferating mammalian cells gradually lose RNAi activity with an increase in the number of cell divisions [12,28,29], we investigated whether cell division occurred in C2C12 cells during the differentiation by means of a BrdU incorporation assay. As shown in Fig. 5A, while the incorporation of BrdU into nuclei could be observed in undifferentiated C2C12 cells, few or no BrdU-positive cells were detectable at day 2 and 7 after induction of the differentiation. In addition, from the data of Fig. 5B, the nature of RNAi activity during the differentiation appears to remain unchanged. Consequently, these observations suggest that C2C12 cells differentiated over 2 days are probably cell-cycle arrested cells, and thus that the decrease in RNAi activity during the myogenic differentiation of C2C12 cells is not caused by cell division.

We further examined RNAi activities in C2C12 myotubes that differentiated for 14 and 21 days. The results indicate that RNAi activities induced by synthetic siRNA duplexes are detectable in those differentiated C2C12 myotubes (Fig. 6), although the transfection efficiency of siRNA and plasmid DNA into the cells seemed to become lower as the culture was long. Taking all the data together, it is conceivable that the decrease in RNAi activity during the myogenic

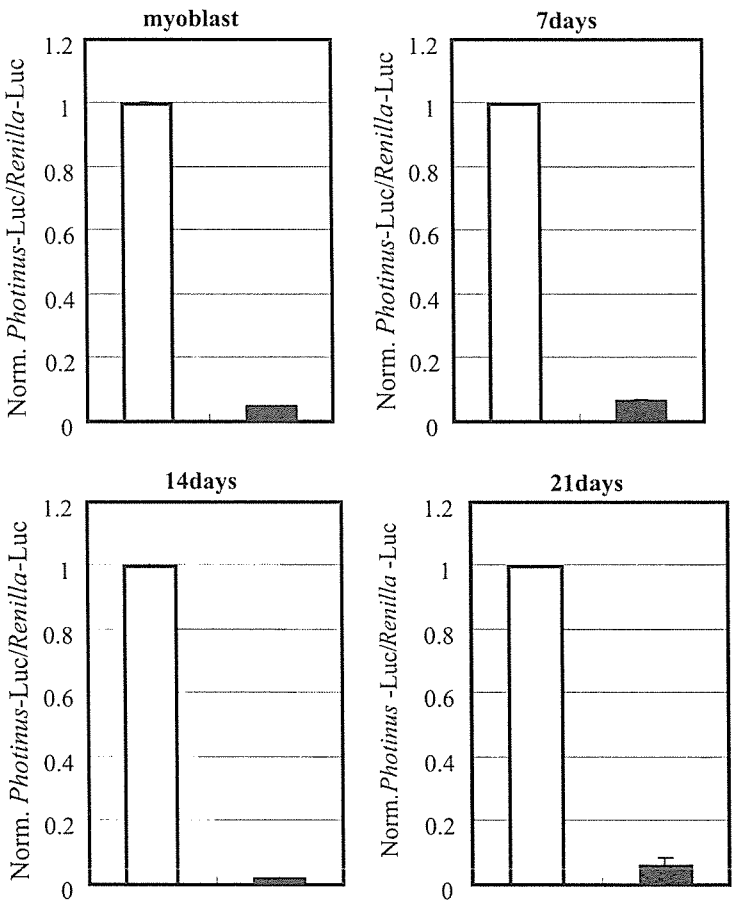

Fig. 6. RNAi induction after myogenic differentiation of C2C12 cells. Myogenic differentiation of C2C12 cells was performed as in Fig. 5. RNAi induction was carried out as in Fig. 2 at indicated days after induction of the myogenic differentiation, and each RNAi activity was examined 24 h after RNAi induction. Ratios of normalised target (*Photinus*) luciferase activity to control (*Renilla*) luciferase activity are indicated as in Fig. 2. Open and solid bars indicate the data in the presence of the non-silencing siRNA and La2 siRNA duplexes, respectively. Data are averages of at least three independent experiments. Error bars represent standard deviations.

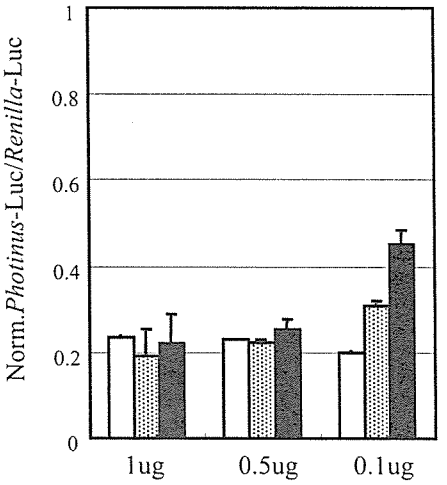

Fig. 7. RNAi induction by short-hairpin RNAs during myogenic differentiation of C2C12 cells. The pRNA-U6.1/Neo/siFluc plasmid (GenScript), which can express a short-hairpin RNA (shRNA) against *Photinus luciferase*, and pRNA-U6.1/Neo empty vector (GenScript) as a control were used. The pGL3-control and phRL-TK plasmids together with a decreasing amount of each of the pRNA-U6.1/Neo/siFluc and pRNA-U6.1/Neo (a negative control) plasmids, from 1 to 0.1 μg, were cotransfected into C2C12 cells. The expression of luciferase was examined 24 h after the transfection. Ratios of normalised target (*Photinus*) luciferase activity to control (*Renilla*) luciferase activity are indicated as in Fig. 2. Open, dotted, and solid bars indicate the data in C2C12 cells that differentiated for 0 (undifferentiated), 2, and 7 days, respectively. Data are averages of at least three independent experiments. Error bars represent standard deviations.

differentiation of C2C12 cell may be caused by losing the stability of functional RISCs in the differentiated C2C12 myotubes.

RNAi induction by short-hairpin RNAs in C2C12 cells

Because Dicer appears to be required for the process of short-hairpin RNAs (shRNAs) into siRNA duplexes, it may be of interest to see if shRNAs can induce RNAi in C2C12 myotubes which barely express *Dicer*. To examine this, we introduced a shRNA expression plasmid against *Photinus* luciferase, pRNA-U6.1/Neo/siRNA, together with the reporter plasmids carrying the *Photinus* and *Renilla* luciferase genes into C2C12 myoblast and myotubes. The results indicate that the shRNA expression plasmid, or shRNAs can induce RNAi in either C2C12 myoblast or myotube (Fig. 7), suggesting that the Dicer protein could be present in those cells. An interesting point to note is that a decrease in the RNAi activity induced by 0.1 μg pRNA-U6.1/Neo/siRNA was observed in C2C12 myotubes that differentiated for 7 days. This may be caused by a possible decrease in the amounts of Dicer and eIF2C1~4 in the cells. To further evaluate the results and a possible relationship between the quantitative level of either Dicer or eIF2C1~4 and RNAi activity, more extensive studies must be conducted.

Integrity of mammalian RNAi

Our previous study has demonstrated that RNAi activity induced by synthetic siRNA duplexes in post mitotic neurons persists for at least 3 weeks, i.e., a long-lasting RNAi activity occurs in mammalian neurons [29]. Our present and previous studies, therefore, suggest that there is a significant difference in the duration of RNAi activity between muscle and neuron, both of which are terminally differentiated and cell cycle-arrested cells. Since neither muscle nor neuron probably undergoes a decrease in the number of functional RISCs by cell division, it may be possible that the stability of functional RISCs could differ between muscle and neuron.

The present observations further suggest the possibility that a little amount of either Dicer or eIF2C1~4 might be sufficient for activation of mammalian RNAi. This seems to be an important point for understanding mammalian RNAi, and further studies on the contribution of either Dicer or eIF2C1~4 to mammalian RNAi must be conducted.

Finally, all the data presented here lead us to the possibility that RNAi may be applicable for a creation of possible model cells and/or model animals for inherited muscular diseases, for example, muscular dystrophy.

Acknowledgments

We thank Drs. Ojima and Takeda (National Institute of Neuroscience) for their technical advice on the preparation of muscle fibers from mouse extensor digitorum longus. This work was supported in part by a Grant-in-Aid from the Japan Society for the Promotion of Science and by research grants from the Ministry of Health, Labor and Welfare in Japan.

References

[1] P.A. Sharp, RNAi and double-strand RNA, Genes Dev. 13 (1999) 139–141.
[2] J.M. Bosher, M. Labouesse, RNA interference: genetic wand and genetic watchdog, Nat. Cell Biol. 2 (2000) E31–E36.
[3] H. Vaucheret, C. Beclin, M. Fagard, Post-transcriptional gene silencing in plants, J. Cell Sci. 114 (2001) 3083–3091.
[4] H. Cerutti, RNA interference: traveling in the cell and gaining functions?, Trends Genet. 19 (2003) 39–46.
[5] S.M. Hammond, E. Bernstein, D. Beach, G.J. Hannon, An RNA-directed nuclease mediates post-transcriptional gene silencing in *Drosophila* cells, Nature 404 (2000) 293–296.
[6] P.D. Zamore, T. Tuschl, P.A. Sharp, D.P. Bartel, RNAi: double-stranded RNA directs the ATP-dependent cleavage of mRNA at 21 to 23 nucleotide intervals, Cell 101 (2000) 25–33.
[7] E. Bernstein, A.A. Caudy, S.M. Hammond, G.J. Hannon, Role for a bidentate ribonuclease in the initiation step of RNA interference, Nature 409 (2001) 363–366.
[8] S.M. Elbashir, W. Lendeckel, T. Tuschl, RNA interference is mediated by 21- and 22-nucleotide RNAs, Genes Dev. 15 (2001) 188–200.

[9] P. Svoboda, P. Stein, H. Hayashi, R.M. Schultz, Selective reduction of dormant maternal mRNAs in mouse oocytes by RNA interference, Development 127 (2000) 4147–4156.
[10] F. Wianny, M. Zernicka-Goetz, Specific interference with gene function by double-stranded RNA in early mouse development, Nat. Cell Biol. 2 (2000) 70–75.
[11] E. Billy, V. Brondani, H. Zhang, U. Muller, W. Filipowicz, Specific interference with gene expression induced by long, double-stranded RNA in mouse embryonal teratocarcinoma cell lines, Proc. Natl. Acad. Sci. USA 98 (2001) 14428–14433.
[12] S. Yang, S. Tutton, E. Pierce, K. Yoon, Specific double-stranded RNA interference in undifferentiated mouse embryonic stem cells, Mol. Cell. Biol. 21 (2001) 7807–7816.
[13] M.R. Player, P.F. Torrence, The 2-5A system: modulation of viral and cellular processes through acceleration of RNA degradation, Pharmacol. Ther. 78 (1998) 55–113.
[14] M. Gale Jr., M.G. Katze, Molecular mechanisms of interferon resistance mediated by viral-directed inhibition of PKR, the interferon-induced protein kinase, Pharmacol. Ther. 78 (1998) 29–46.
[15] S.M. Elbashir, J. Harborth, W. Lendeckel, A. Yalcin, K. Weber, T. Tuschl, Duplexes of 21-nucleotide RNAs mediate RNA interference in cultured mammalian cells, Nature 411 (2001) 494–498.
[16] S. Matsuda, Y. Ichigotani, T. Okuda, T. Irimura, S. Nakatsugawa, M. Hamaguchi, Molecular cloning and characterization of a novel human gene (HERNA) which encodes a putative RNA-helicase, Biochim. Biophys. Acta 1490 (2000) 163–169.
[17] R.H. Nicholson, A.W. Nicholson, Molecular characterization of a mouse cDNA encoding Dicer, a ribonuclease III ortholog involved in RNA interference, Mamm. Genome 13 (2002) 67–73.
[18] P. Provost, D. Dishart, J. Doucet, D. Frendewey, B. Samuelsson, O. Radmark, Ribonuclease activity and RNA binding of recombinant human Dicer, EMBO J. 21 (2002) 5864–5874.
[19] H. Zhang, F.A. Kolb, V. Brondani, E. Billy, W. Filipowicz, Human Dicer preferentially cleaves dsRNAs at their termini without a requirement for ATP, EMBO J. 21 (2002) 5875–5885.
[20] K.S. Yan, S. Yan, A. Farooq, A. Han, L. Zeng, M.M. Zhou, Structure and conserved RNA binding of the PAZ domain, Nature 426 (2003) 468–474.
[21] J. Martinez, A. Patkaniowska, H. Urlaub, R. Luhrmann, T. Tuschl, Single-stranded antisense siRNAs guide target RNA cleavage in RNAi, Cell 110 (2002) 563–574.
[22] N. Doi, S. Zenno, R. Ueda, H. Ohki-Hamazaki, K. Ui-Tei, K. Saigo, Short-interfering-RNA-mediated gene silencing in mammalian cells requires Dicer and eIF2C translation initiation factors, Curr. Biol. 13 (2003) 41–46.
[23] J.D. Rosenblatt, A.I. Lunt, D.J. Parry, T.A. Partridge, Culturing satellite cells from living single muscle fiber explants, In Vitro Cell. Dev. Biol. Anim. 31 (1995) 773–779.
[24] D. Yaffe, O. Saxel, Serial passaging and differentiation of myogenic cells isolated from dystrophic mouse muscle, Nature 270 (1977) 725–727.
[25] H. Hohjoh, RNA interference (RNAi) induction with various types of synthetic oligonucleotide duplexes in cultured human cells, FEBS Lett. 521 (2002) 195–199.
[26] S.M. Hammond, S. Boettcher, A.A. Caudy, R. Kobayashi, G.J. Hannon, Argonaute2, a link between genetic and biochemical analyses of RNAi, Science 293 (2001) 1146–1150.
[27] R.W. Williams, G.M. Rubin, ARGONAUTE1 is required for efficient RNA interference in *Drosophila* embryos, Proc. Natl. Acad. Sci. USA 99 (2002) 6889–6894.
[28] T. Holen, M. Amarzguioui, M.T. Wiiger, E. Babaie, H. Prydz, Positional effects of short interfering RNAs targeting the human coagulation trigger tissue factor, Nucleic Acids Res. 30 (2002) 1757–1766.
[29] K. Omi, K. Tokunaga, H. Hohjoh, Long-lasting RNAi activity in mammalian neurons, FEBS Lett. 558 (2004) 89–95.

Available online at www.sciencedirect.com
SCIENCE DIRECT®
Analytical Biochemistry 347 (2005) 106–111
ANALYTICAL BIOCHEMISTRY
www.elsevier.com/locate/yabio

More than a 100-fold increase in immunoblot signals of laser-microdissected inclusion bodies with an excessive aggregation property by oligomeric actin interacting protein 2/D-lactate dehydrogenase protein 2

Naomi S. Hachiya [a], Takuya Ohkubo [b], Yoshimichi Kozuka [c], Mineo Yamazaki [d], Osamu Mori [e], Hidehiro Mizusawa [b], Yuji Sakasegawa [f], Kiyotoshi Kaneko [a,*]

[a] *Second Department of Physiology, Tokyo Medical University, Shinjuku-ku, Tokyo 160-8402, Japan*
[b] *Department of Neurology and Neurological Science, Graduate School of Medicine, Tokyo Medical and Dental University, Bunkyo-ku, Tokyo 113-0034, Japan*
[c] *Ultrastructural Research, National Institute of Neuroscience, National Center of Neurology and Psychiatry, Kodaira, Tokyo 187-8502, Japan*
[d] *Department of Neurology and Nephrology, Nippon Medical School, Bunkyo-ku, Tokyo 113-8602, Japan*
[e] *Second Department of Pathology, Nippon Medical School, Bunkyo-ku, Tokyo 113-8602, Japan*
[f] *Division of Prion Protein Biology, Department of Prion Protein Research, Graduate School of Medicine, Tohoku University, Aoba-ku, Sendai 980-8575, Japan*

Received 6 July 2005
Available online 26 September 2005

Abstract

We established a histobiochemical approach targeting micron-order inclusion bodies possessing extensive aggregation properties in situ by using a nonchemical denaturant (oligomeric actin interacting protein 2/D-lactate dehydrogenase protein 2 [Aip2p/Dld2p]) with the combinatorial method of laser-microdissection and immunoblot analysis. As a model, pick bodies were chosen and laser-microdissected from three different brain regions of two patients with Pick's disease. Initially, 500 to 2000 pick bodies were applied onto SDS–PAGE gels after boiling in Laemmli's sample buffer according to established immunoblotting procedures; however, only faint signals were obtained. Following negative results with chemical denaturants or detergent, including 6 M guanidine hydrochloride, 8 M urea, and 2% SDS, the laser-microdissected pick bodies were pretreated with oligomeric Aip2p/Dld2p, which possesses robust protein unfolding activity under biological conditions. Strikingly, only one pick body was sufficient to illustrate an immunoblot signal, indicating that pretreatment with oligomeric Aip2p/Dld2p enhanced the immunoblot sensitivity by more than 100-fold. Pretreatment with oligomeric Aip2p/Dld2p also allowed us to quantify the total protein content of pick bodies. Thus, use of oligomeric Aip2p/Dld2p significantly contributed toward the acquisition of information pertaining to the molecular profile of proteins possessing an extensive aggregation property, particularly in small amounts.

Keywords: Oligomeric Aip2p/Dld2p; Protein conformation unfolding activity; Laser-microdissection; Inclusion bodies; Pick bodies; Phosphorylated tau

While immunohistochemical analysis has been widely used for the characterization of microstructures under various conditions and of disorders at a light microscopic level, immunoblot analysis has been indispensable in the analysis of proteins at a macroscopic level [1]. Currently, no analytical methods equivalent to the immunoblot have been developed against targets for examination under the microscope, although the recent development of a laser-microdissection methodology allows us to manipulate microstructures at microscopic regions of interest in situ [2].

* Corresponding author. Fax: +81 3 3351 6544.
E-mail address: k-kaneko@tokyo-med.ac.jp (K. Kaneko).

0003-2697/$ - see front matter © 2005 Elsevier Inc. All rights reserved.
doi:10.1016/j.ab.2005.09.004

Against this backdrop, we developed a novel combinatorial method that uses laser-microdissection and immunoblotting to allow the characterization of the molecular profile of proteins at microscopic regions of interest. As a model, we examined brain samples of Pick's disease, a type of progressive presenile dementia that affects brain function, eventually causing loss of verbal skills and problem-solving ability [3]. Pick's disease accounts for 5% of all dementias and is characterized neuropathologically by distinct tau-immunoreactive intraneuronal inclusions known as pick bodies [4]. Abnormally phosphorylated tau proteins were detected from total brain homogenates [4–6], but no investigation has been reported with isolated pick bodies to date.

Given limited sample availability and the absence of in vitro amplification steps for proteins, use of laser-microdissected samples depends largely on highly sensitive protein detection methods [7]. Furthermore, these inclusion bodies generally possess extensive aggregation properties that often negatively affect the immunoblot assay. Unfortunately, use of conventional procedures, including sample pretreatment with chemical denaturing agents or detergent, was ineffective. In an effort to overcome the problem, oligomeric actin interacting protein 2 (Aip2p)[1] [8]/D-lactate dehydrogenase protein 2 (Dld2p) [9,10] was used as a non-chemical denaturant [11–13]. Dld2p [9,10] was initially identified as Aip2p using a two-hybrid screen to search for proteins that interact with actin [8]. During our search for protein conformation unfolding activity, we further identified oligomeric Aip2p/Dld2p isolated from *Saccharomyces cerevisiae* as exhibiting robust protein conformation unfolding activity [11]. Oligomeric Aip2p/Dld2p possesses a unique grapple-like structure with an ATP-dependent opening that is required for protein conformation unfolding activity [12,13]. In the presence of 1 mM ATP or AMP–PNP, oligomeric Aip2p/Dld2p bound to all substrates so far examined and subsequently modified the protein conformation. Furthermore, oligomeric Aip2p/Dld2p was able to modify the conformation of pathogenic highly aggregated polypeptides such as recombinant prion protein (rPrP) in the beta form, alpha-synuclein, and Abeta (1–42) in the presence of ATP in vitro [13]. This procedure consists simply of combining oligomeric Aip2p/Dldp2 and 1 mM ATP in a reaction tube containing the collected pick bodies and then incubating the sample for 60 min at 30 °C.

Oligomeric Aip2p/Dld2p significantly increases the immunoblot signals by more than 100-fold. The histobiochemical approach detailed in this study allows us to analyze single pick bodies in the order of several micrometers in radius.

[1] *Abbreviations used*: Aip2p, actin interacting protein 2; Dld2p, D-lactate dehydrogenase protein 2; rPrP, recombinant prion protein; BSA, bovine serum albumin; EGTA, ethyleneglycotetraacetic acid; TCA, trichloroacetic acid; PBS, phosphate-buffered saline; PBS-T, PBS containing 0.05% Tween 20; TBH, total brain homogenate; LC–MS/MS, liquid chromatography–tandem mass spectrometry.

Materials and methods

After informed consent had been obtained, frontal (Y337F and Y332F) and temporal (Y332T) cortexes from two patients with sporadic Pick's disease (patient 1 (Y337): female, 71 years old; patient 2 (Y332): male, 72 years old) were placed in a deep freezer (−80 °C) at Nippon Medical School until use. The procedures followed were in accordance with the institutional ethical standards on human experimentation.

Oligomeric Aip2p/Dld2p was expressed and purified as described previously [11,12]. Anti-tau AT8 (phosphorylation-dependent monoclonal antibody specific to phosphorylated Ser202/Thr205) and AT100 (specific to phosphorylated Thr212/Ser214) were purchased from Innogenetics. Anti-Aip2p/Dld2p antibody was raised against the synthetic peptide corresponding to the C-terminal 15 amino acid residues of Aip2p (VHYDPNGILNPYKYI) that were coupled through a COOH-terminal cysteine residue to bovine serum albumin (BSA) [11].

Slide preparations were made using a NexES Automated Immunohistochemistry Staining System (Ventana Medical Systems) with 1:200 AT8. Immunostained pick bodies (10–15 μm in diameter) (Table 1) were dissected using a Laser Microdissection System (Olympus Optical) coupled to a Hoya laser cutter (HCL2100, 30 mJ/pulse, 266 nm). Dissected samples were collected using a Cell Tram Oil hydraulic manual microinjector (Eppendorf) with distilled water.

Immunoblot analyses were performed as follows. First, total brain homogenates (10–40 μg) or laser-dissected pick bodies (500 pieces) were solubilized in 500 μl of ice-cold extraction buffer (Tris–chloride [pH 7.4], 0.8 M NaCl, 1 mM ethyleneglycotetraacetic acid [EGTA], 10% sucrose, and 1/1000 [w/v] protease inhibitor cocktail [Sigma] with 1% sodium *N*-lauroyl sarcosinate [sarkosyl]). Sarkosyl-insoluble fractions were collected by centrifugation at 182,000*g* for 30 min at 4 °C and then suspended in 50 mM Tris–chloride (pH 7.4). Samples were pretreated with 8 M urea (Wako Chemicals), 6 M guanidine hydrochloride (Nacalai Tesque), or 2% SDS (Wako Chemicals), followed by trichloroacetic acid (TCA) precipitation in an effort to denature or untangle the samples. Pretreatment with Aip2p/Dld2p was performed as described previously

Table 1
Quantitative analyses of pick bodies

	Y332T	Y332F	Y337F
Total protein (ng/pick body)	0.8	1.1	2.8
Average diameter (μm)	10	10	15
SRelative density	1.6	2.2	1.6

Note. The protein concentration of sarkosyl-insoluble fractions was measured following pretreatment with oligomeric Aip2p/Dld2p, and the relative density of the pick bodies was calculated. Frontal (Y337F and Y332F) and temporal (Y332T) cortexes from two patients with sporadic Pick's disease (patient 1 (Y337): female, 71 years old; patient 2 (Y332): male, 72 years old) were analyzed.

[11–13]. Briefly, 1 to 500 ng of oligomeric Aip2p/Dld2p was mixed with the sarkosyl-insoluble fraction of 1 to 500 pick bodies at a ratio of 1 ng per 1 pick body in the presence of 1 mM ATP for 60 min at 30 °C in a total volume of 20 μl. Samples were then loaded onto 12% SDS–PAGE gels and transferred onto 0.22-μm nitrocellulose membranes in 25 mM Tris–190 mM glycine–0.01% SDS–20% methanol at 400 mA for 40 min at 4 °C. Membranes were blocked using 4% BSA in phosphate-buffered saline (PBS) containing 0.05% Tween 20 (PBS-T), incubated with 1:1000 (unless otherwise indicated) AT8 and AT100 in PBS-T overnight at 4 °C, washed with PBS-T several times at room temperature, and then incubated with 1:10,000 horseradish peroxidase-conjugated anti-mouse IgG antibody (Amersham) in PBS-T for 1 h at room temperature. After washing the membranes, the immunodecorated bands were visualized using ECL-plus (Amersham) and then analyzed using a Fluor-S MAX MultiImager or VersaDoc (Bio-Rad Laboratories).

The protein concentration of the pick bodies pretreated with oligomeric Aip2p/Dld2p was measured using a spectrophotometer (Tecan) at 595 nm in combination with a Protein Assay System (Bio-Rad Laboratories) according to the manufacturers' instructions. Oligomeric Aip2p/Dld2p was applied at a ratio of 1 ng per 1 pick body, and the value was subtracted afterward.

Results

The laser-microdissection system combined with the sample collector facilitated the dissection of targets (Fig. 1A). Up to 500 pick bodies were collected each time over a period of 1 day. Initially, 500 pick bodies were applied onto SDS–PAGE gels after boiling in Laemmli's sample buffer according to established immunoblotting procedures [1]. However, only faint and blurred signals were obtained with anti-tau antibodies AT8 and AT100 (Fig. 1B, lane 4) in comparison with 10 to 40 μg of total brain homogenate (TBH, Fig. 1B, lanes 2 and 3). Immunostaining of the entire gel, including the loading wells and the stacking gel, revealed no additional immunoblot signals that may have arisen from the extensive aggregation property of the pick bodies. Further increases in the number of pick bodies applied (up to 2000) could not improve the signal intensity (data not shown).

The effect of chemical denaturants or detergent, including 6 M guanidine hydrochloride, 8 M urea, and 2% SDS,

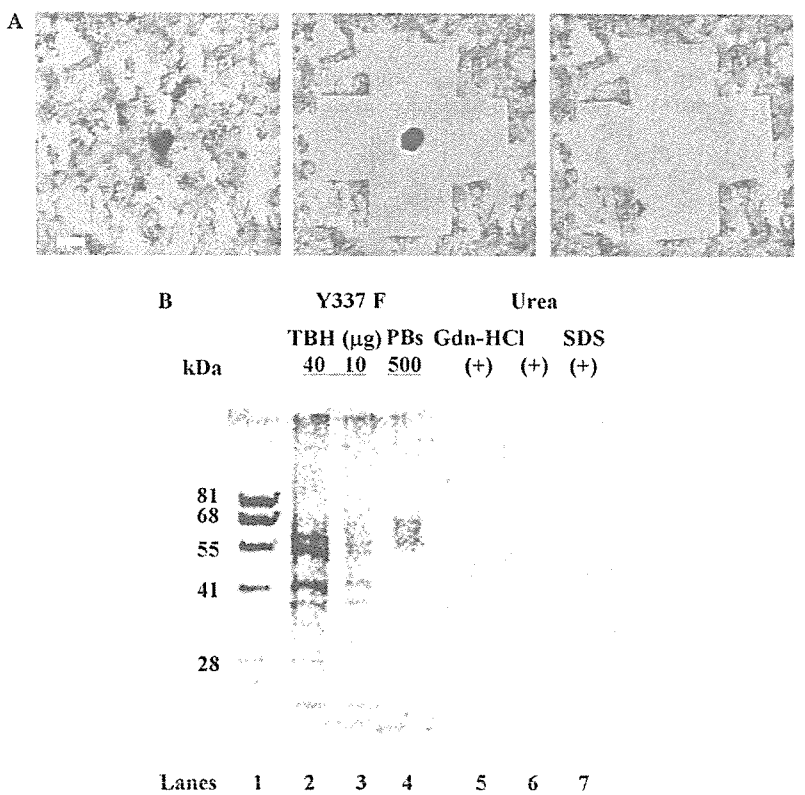

Fig. 1. Immunological analyses of laser-microdissected pick bodies (PBs). (A) Left panel: 5-μm-thick cryosection. PBs of frontal cortex from patient Y337 (Y337F) are stained with AT8 (1:200, purple) and hematoxylin (blue). Middle and right panels: PBs isolated from the section using a laser-microdissector. Scale bar is 10 μm. (For interpretation of the references to color in this figure legend, the reader is referred to the Web version of this article.) (B) Immunoblot analyses of PBs pretreated with chemical denaturants or detergent. Approximately 500 PBs were used for each trial. Lane 1: molecular weight marker (Dr. Western, Oriental Yeast); lanes 2 and 3: total brain homogenate (TBH) of Y337F (40 and 10 μg, respectively); lanes 4 to 7: 500 laser-microdissected PBs of Y337F with no pretreatment (lane 4), 6 M guanidine hydrochloride (Gdn-HCl, lane 5), 8 M urea (lane 6), and 2% SDS pretreatment (lane 7). Samples were stained with anti-tau AT8 (1:1000) and AT100 (1:1000).

was then determined. Use of the aforementioned chaotropic agents, however, resulted in no improvement of immunoblot signals (Fig. 1B, lanes 5–7). In fact, the signal intensities diminished somewhat, possibly due to the presence of phosphorylated tau bound to the walls of the tube after removing the chaotropic agents prior to loading onto the SDS–PAGE gels [14].

Although negative results were obtained following use of the aforementioned chemical denaturants and detergent, we demonstrated that oligomeric Aip2p/Dld2p could modify the conformation of pathogenic highly aggregated polypeptides such as rPrP in the beta form, alpha-synuclein, and Abeta (1–42) in the presence of ATP [13]. Hence, the pick bodies were pretreated with oligomeric Aip2p/Dld2p prior to loading onto SDS–PAGE gels. Surprisingly, immunoblot analyses of Y337F, Y332F, and Y332T demonstrated discrete bands stained with anti-tau AT8 and AT100 antibodies following pretreatment with oligomeric Aip2p/Dld2p (Fig. 2). In a serial dilution assay, 1/500 of 500 pick bodies (equivalent to 1 pick body) was detected (Fig. 2, upper panel, lanes 4–8; lower panel, lanes 2–10).

These immunoreactive bands migrated slightly faster than those associated with the 500 pick bodies processed without oligomeric Aip2p/Dld2p pretreatment (Fig. 2, upper panel, lane 2). One possible explanation is that pretreatment with oligomeric Aip2p/Dld2p might allow the detection of the phosphorylated form of 60 kDa tau (tau 60) [4–6], whereas only the phosphorylated form of 69 kDa tau (tau 69) is negligibly detected following boiling in Laemmli's sample buffer according to classical immunoblotting procedures. Whether the different tau isoform could account for the faster migration pattern observed remains to be determined.

Oligomeric Aip2p/Dld2p was also detected in the same reaction mixtures using anti-Aip2p/Dld2p antibody (Fig. 2, upper panel, lanes 12–16) but did not cross-react with anti-tau AT8 and AT100 antibodies (Fig. 2, upper panel, lane 10). It should be noted that a single pick body directly pretreated with oligomeric Aip2p/Dld2p was sufficient to yield an immunoblot signal (Fig. 2, lower panel, lane 13), indicating that pretreatment with oligomeric Aip2p/Dld2p enhanced the immunoblot signal by more than 100-fold. Transmission electron microscopy with uranyl acetate negative staining of laser-microdissected pick bodies (Fig. 3) revealed that they were untangled following treatment with oligomeric Aip2p/Dld2p, whereas the

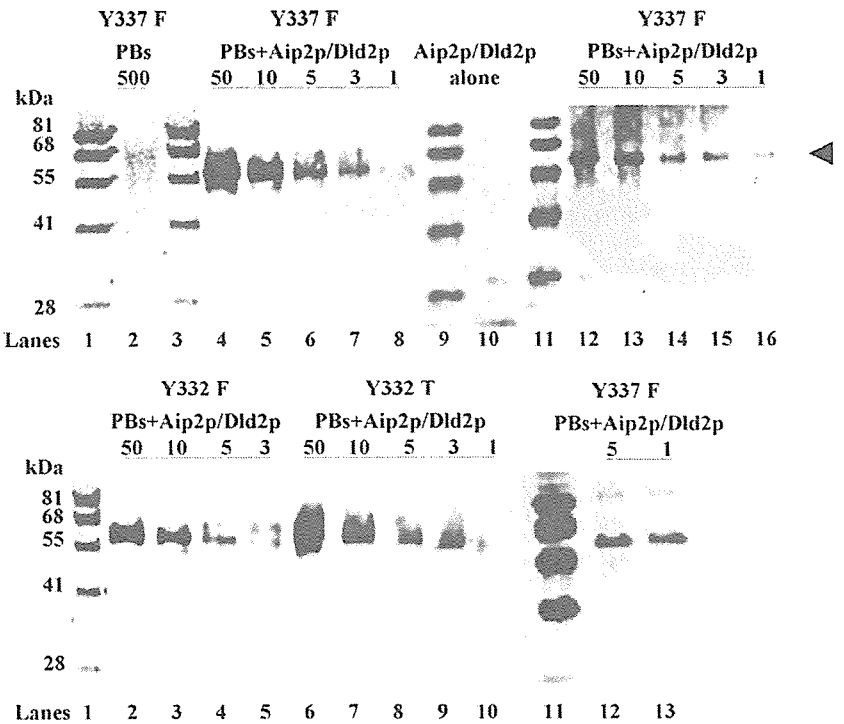

Fig. 2. Immunoblot analyses of laser-microdissected pick bodies (PBs) from Y337F (frontal cortex), Y332F (frontal cortex), and Y332T (temporal cortex). Upper panels: Molecular weight marker (Dr. Western, Oriental Yeast, lanes 1, 3, 9, and 11), 500 laser-microdissected PBs of Y337F (lane 2), and serial dilutions equivalent to 50, 10, 5, and 3 PBs and 1 PB of Y337F (lanes 4–8 and 12–16). Lane 2 represents sample without oligomeric Aip2p/Dld2p pretreatment, whereas lanes 4 to 8 and lanes 12 to 16 represent samples with oligomeric Aip2p/Dld2p pretreatment. Lane 10: 50 ng of Aip2p/Dld2p alone. Lanes 2, 4 to 8, and 10 were stained with anti-tau AT8 (1:1000) and AT100 (1:1000), whereas lanes 12 to 16 were stained with anti-Aip2p/Dld2p polyclonal antibody. The arrowhead indicates the position of Aip2p/Dld2p (MW = 58 kDa). Lower panels: Molecular weight marker (Dr. Western, Oriental Yeast, lanes 1 and 11), serial dilutions of 500 PBs of Y332F equivalent to 50, 10, 5, and 3 PBs (lanes 2–5), and those of Y332T equivalent to 50, 10, 5, and 3 PBs and 1 PB (lanes 6–10). Lanes 12 and 13: 5 PBs and 1 PB of Y337F, respectively. Samples in lower panels were pretreated with oligomeric Aip2p/Dld2p and stained with anti-tau AT8 (1:1000) and AT100 (1:1000).

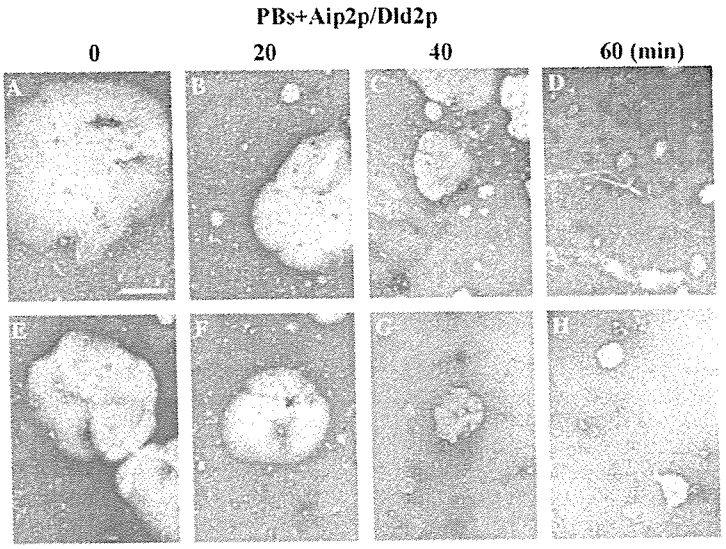

Fig. 3. Transmission electron microscopy with uranyl acetate negative staining of laser-microdissected pick bodies (PBs) prior to (A and E) and following oligomeric Aip2p/Dld2p pretreatment for 20 min (B and F), 40 min (C and G), and 60 min (D and H). For the negative staining, 500 PBs of Y332F were used as specimens. Scale bar is 4 μm.

average diameter of pick bodies decreased markedly, from 10 to 15 μm to less than 1 μm, in a time-dependent manner.

Although protein quantification of highly aggregated proteins such as pick bodies has been quite problematic to date, pretreatment with oligomeric Aip2p/Dld2p allows the ready quantification of the protein content of pick bodies (Table 1). The protein concentrations of sarkosyl-insoluble fractions were 0.8 ng (Y332T), 1.1 ng (Y332F), and 2.8 ng (Y337F) per 1 pick body. Because the average diameters of the pick bodies were 10 μm (Y332) and 15 μm (Y337), the relative densities of the pick bodies were 1.6 to 2.2 (Y332) and 1.6 (Y337).

Discussion

Our novel combinatorial method targets proteins relating to specific regions of interest at the micrometer order and exclusively allows the gathering of information pertaining to the molecular profile, such as molecular weight, of target proteins under the microscope in situ. During our investigations, we noticed that laser-microdissected pick bodies exhibited only faint and blurred immunoblot signals with anti-tau AT8 and AT100 antibodies, even following pretreatment with chemical denaturants or detergent, presumably resulting from the extensive aggregation property. In fact, this is extremely crucial when only a minimal quantity of target protein is available.

The protein conformation unfolding activity of oligomeric Aip2p/Dld2p can modify the conformation of pathogenic highly aggregated polypeptides [13]. Therefore, pick bodies were pretreated with oligomeric Aip2p/Dld2p to overcome the extensive aggregation property. With the pretreatment, 500 ng of oligomeric Aip2p/Dld2p (MW ~700 kDa) was mixed with 500 pick bodies consisting of abnormally phosphorylated tau (MW = 58 kDa), indicating that the stoichiometry of oligomeric Aip2p/Dld2p:phosphorylated tau is approximately 1:10. As shown in Fig. 2, oligomeric Aip2p/Dld2p pretreatment enhanced the immunoblot signals by more than 100-fold.

The inclusion bodies, which might protect against toxicity [15], have been associated with various protein conformation disorders, including Alzheimer's disease [16], Parkinson's disease [17], and prion disease (e.g., bovine spongiform encephalopathy) [18]. Actually, the robust protein conformation unfolding activity of oligomeric Aip2p/Dld2p modulated the conformation of Abeta (1–42) peptide associated with Alzheimer's disease, alpha-synuclein associated with Parkinson's disease, and rPrP in the beta form associated with prion disease in vitro [13]. Therefore, use of oligomeric Aip2p/Dld2p with our combinatorial method provides significant improvement in the investigation of normal or abnormal microstructures under various conditions and of disorders with extremely enhanced sensitivity.

Making use of this unprecedented property of oligomeric Aip2p/Dld2p may yield further potential applications. For example, a number of proteomic strategies rely on liquid chromatography–tandem mass spectrometry (LC–MS/MS), but sample preparation methods typically involve the use of detergents and chaotropic agents that often interfere with chromatographic separation and/or electrospray ionization [19]. Use of oligomeric Aip2p/Dld2p, however, would not interfere with the LC–MS/MS procedures and might even prove to be ideal for sample pretreatment. Overall, use of oligomeric Aip2p/Dld2p might significantly facilitate nano-scale analysis, which is often hindered by the aggregation property of target proteins present under various analytical conditions, especially when the sample protein is present in minor quantities.

Acknowledgments

We thank K. Watanabe and K. Takayama for technical assistance. This work was supported by grants from the Ministry of Health, Labor, and Welfare and the Ministry of Education, Culture, Sports, Science, and Technology, Japan, and from the Core Research for Evolutional Science and Technology (CREST) of Japan Science and Technology Agency.

References

[1] U.K. Laemmli, Cleavage of structural proteins during the assembly of the head of bacteriophage T4, Nature 227 (1970) 680–685.
[2] T. Tanaka, T. Ito, M. Furuta, C. Eguchi, H. Toda, E. Wakabayashi-Takai, K. Kaneko, In situ phage screening: a method for identification of subnanogram tissue components in situ, J. Biol. Chem. 277 (2002) 30382–30387.
[3] S. Hardin, B. Schooley, A story of Pick's disease: a rare form of dementia, J. Neurosci. Nurs. 34 (2002) 117–122.
[4] V. Zhukareva, D. Mann, S. Pickering-Brown, K. Uryu, T. Shuck, K. Shah, M. Grossman, B.L. Miller, C.M. Hulette, S.C. Feinstein, J.Q. Trojanowski, V.M. Lee, Sporadic Pick's disease: a tauopathy characterized by a spectrum of pathological tau isoforms in gray and white matter, Ann. Neurol. 51 (2002) 730–739.
[5] A. Delacourte, N. Sergeant, A. Wattez, D. Gauvreau, Y. Robitaille, Vulnerable neuronal subsets in Alzheimer's and Pick's disease are distinguished by their tau isoform distribution and phosphorylation, Ann. Neurol. 43 (1998) 193–204.
[6] T. Arai, K. Ikeda, H. Akiyama, Y. Shikamoto, K. Tsuchiya, S. Yagishita, T. Beach, J. Rogers, C. Schwab, P.L. McGeer, Distinct isoforms of tau aggregated in neurons and glial cells in brains of patients with Pick's disease, corticobasal degeneration, and progressive supranuclear palsy, Acta Neuropathol. (Berl.) 101 (2001) 167–173.
[7] W. Martinet, V. Abbeloos, N. Van Acker, G.R. De Meyer, A.G. Herman, M.M. Kockx, Western blot analysis of a limited number of cells: a valuable adjunct to proteome analysis of paraffin wax-embedded, alcohol-fixed tissue after laser capture microdissection, J. Pathol. 202 (2004) 382–388.
[8] D.C. Amberg, E. Basart, D. Botstein, Defining protein interactions with yeast actin in vivo, Nat. Struct. Biol. 2 (1995) 28–35.
[9] A. Chelstowska, Z. Liu, Y. Jia, D. Amberg, R.A. Butow, Signalling between mitochondria and the nucleus regulates the expression of a new D-lactate dehydrogenase activity in yeast, Yeast 15 (1999) 1377–1391.
[10] M.J. Flick, S.F. Konieczny, Identification of putative mammalian D-lactate dehydrogenase enzymes, Biochem. Biophys. Res. Commun. 295 (2002) 910–916.
[11] N.S. Hachiya, Y. Sakasegawa, A. Jozuka, S. Tsukita, K. Kaneko, Interaction of D-lactate dehydrogenase protein 2 (Dld2p) with F-actin: Implication for an alternative function of Dld2p, Biochem. Biophys. Res. Commun. 319 (2004) 78–82.
[12] N.S. Hachiya, Y.H.S. Sakasegawa, A. Jozuka, S. Tsukita, K. Kaneko, Oligomeric Aip2p/Dld2p forms a novel grapple-like structure and has an ATP-dependent F-actin conformation modifying activity in vitro, Biochem. Biophys. Res. Commun. 320 (2004) 1271–1276.
[13] N.S. Hachiya, Y.H.S. Sakasegawa, A. Jozuka, S. Tsukita, K. Kaneko, Oligomeric Aip2p/Dld2p modifies the protein conformation of both properly-folded and misfolded substrates in vitro, Biochem. Biophys. Res. Commun. 323 (2004) 339–344.
[14] K. Kaneko, D. Peretz, K.M. Pan, T.C. Blochberger, H. Wille, R. Gabizon, O.H. Griffith, F.E. Cohen, M.A. Baldwin, S.B. Prusiner, Prion protein (PrP) synthetic peptides induce cellular PrP to acquire properties of the scrapie isoform, Proc. Natl. Acad. Sci. USA 92 (1995) 11160–11164.
[15] M. Tanaka, Y.M. Kim, G. Lee, E. Junn, T. Iwatsubo, M.M. Mouradian, Aggresomes formed by alpha-synuclein and synphilin-1 are cytoprotective, J. Biol. Chem. 279 (2004) 4625–4631.
[16] J.W. Lustbader, M. Cirilli, C. Lin, H.W. Xu, K. Takuma, N. Wang, C. Caspersen, X. Chen, S. Pollak, M. Chaney, F. Trinchese, S. Liu, F. Gunn-Moore, L.F. Lue, D.G. Walker, P. Kuppusamy, Z.L. Zewier, O. Arancio, D. Stern, S.S. Yan, H. Wu, ABAD directly links Abeta to mitochondrial toxicity in Alzheimer's disease, Science 304 (2004) 448–452.
[17] J.T. Greenamyre, T.G. Hastings, Parkinson's: divergent causes, convergent mechanisms, Science 304 (2004) 1120–1122.
[18] M.P. Mayer, H. Schroder, S. Rudiger, K. Paal, T. Laufen, B. Bukau, Multistep mechanism of substrate binding determines chaperone activity of Hsp70, Nat. Struct. Biol. 7 (2000) 586–593.
[19] J. Blonder, M.B. Goshe, R.J. Moore, L. Pasa-Tolic, C.D. Masselon, M.S. Lipton, R.D. Smith, Enrichment of integral membrane proteins for proteomic analysis using liquid chromatography–tandem mass spectrometry, J. Proteome Res. 1 (2002) 351–360.

Available online at www.sciencedirect.com
SCIENCE DIRECT®
Neuroscience Letters 374 (2005) 98–103
Neuroscience Letters
www.elsevier.com/locate/neulet

Mitochondrial localization of cellular prion protein (PrP^C) invokes neuronal apoptosis in aged transgenic mice overexpressing PrP^C

Naomi S. Hachiya[a,b], Makiko Yamada[a,b], Kota Watanabe[a,b], Akiko Jozuka[a,b], Takuya Ohkubo[a,c], Kenichi Sano[a,1], Yoshio Takeuchi[a,2], Yoshimichi Kozuka[d], Yuji Sakasegawa[a], Kiyotoshi Kaneko[a,b,*]

[a] *Departments of a Cortical Function Disorders, National Institute of Neuroscience (NIN), National Center of Neurology and Psychiatry (NCNP), Kodaira, Tokyo 187-8502, Japan*
[b] *Core Research for Evolutional Science and Technology (CREST), Japan Science and Technology Agency, Kawaguchi, Saitama 332-0012, Japan*
[c] *Department of Neurology and Neurological Science, Graduate School of Medicine, Tokyo Medical and Dental University, Bunkyo-ku, Tokyo 113-0034, Japan*
[d] *Ultrastructural Research, National Institute of Neuroscience (NIN), National Center of Neurology and Psychiatry (NCNP), Kodaira, Tokyo 187-8502, Japan*

Received 14 September 2004; received in revised form 12 October 2004; accepted 13 October 2004

Abstract

Recent studies suggest that the disease isoform of prion protein (PrP^{Sc}) is non-neurotoxic in the absence of cellular isoform of prion protein (PrP^C), indicating that PrP^C may participate directly in the neurodegenerative damage by itself. Meanwhile, transgenic mice harboring a high-copy-number of wild-type mouse (Mo) PrP^C develop a spontaneous neurological dysfunction in an age-dependent manner, even without inoculation of PrP^{Sc} and thus, investigations of these aged transgenic mice may lead to the understanding how PrP^C participate in the neurotoxic property of PrP. Here we demonstrate mitochondria-mediated neuronal apoptosis in aged transgenic mice overexpressing wild-type $MoPrP^C$ (Tg(MoPrP)4053/FVB). The aged mice exhibited an aberrant mitochondrial localization of PrP^C concomitant with decreased proteasomal activity, while younger littermates did not. Such aberrant mitochondrial localization was accompanied by decreased mitochondrial manganese superoxide dismutase (Mn-SOD) activity, cytochrome *c* release into the cytosol, caspase-3 activation, and DNA fragmentation, most predominantly in hippocampal neuronal cells. Following cell culture studies confirmed that decrease in the proteasomal activity is fundamental for the PrP^C-related, mitochondria-mediated apoptosis. Hence, the neurotoxic property of PrP^C could be explained by the mitochondria-mediated neuronal apoptosis, at least in part.

Keywords: PrP^C; Proteasomal activity; Mitochondrial localization; Superoxide dismutase activity; Mitochondria-mediated apoptosis

The posttranslational conformational change of the cellular isoform of prion protein (PrP^C) into its scrapie isoform (PrP^{Sc}) is the fundamental process underlying the pathogenesis of prion diseases [24], but the molecular events through which prion infection and the resulting accumulation of PrP lead to the neuronal dysfunction, vacuolation, and death that characterize prion pathology remain unclear [6].

Importantly, PrP^{Sc}, the disease isoform of PrP, seems to be non-neurotoxic in the absence of PrP^C, suggesting that PrP^C may participate directly in the prion neurodegenerative damage by itself, and the cellular pathways activated by neurotoxic forms of PrP that ultimately result in neuronal death are also being investigated, and several possible mechanisms have been uncovered [6]. For example, cross-linking

* Corresponding author. Tel.: +81 42 346 1718; fax: +81 42 346 1748.
E-mail address: kaneko@ncnp.go.jp (K. Kaneko).
[1] Present address: Hinoicda Kagaku Ltd., Hino-city, Tokyo 191-0061, Japan.
[2] Present address: KOHJIN-BIO Ltd., Sakado-city, Saitama 350-0214, Japan.

0304-3940/$ – see front matter © 2004 Elsevier Ireland Ltd. All rights reserved.
doi:10.1016/j.neulet.2004.10.044

PrP^C in vivo with specific monoclonal antibodies was found to trigger neuronal apoptosis, suggesting that PrP^C functions in the control of neuronal survival [26]. In fact, neural tissues overexpressing PrP^C grafted into the brains of PrP^C-deficient mice develop the severe histopathological changes characteristic of prion disease when infected with prions, but no pathological changes were seen in PrP^C-deficient tissue, not even in the immediate vicinity of the grafts despite the presence of high levels of PrP^{Sc} [2]. In addition, interruption of PrP^C expression during an ongoing prion infection prevents neuronal loss and reverses early spongiform change [16]. The continued accumulation of PrP^{Sc} in this model after neuronal PrP^C depletion is likely to reflect prion replication predominantly in both microglia and astrocytes glial cells without PrP^C depletion, which support PrP^{Sc} replication. The PrP^{Sc} deposits colocalize with astrocytes in the brains of infected mice with neuronal PrP^C depletion, which was not seen in scrapie-infected control animals without PrP depletion. The fact that these mice remain asymptomatic indicates that even extensive extraneuronal PrP^{Sc} replication does not cause clinical disease or neurodegeneration in this model. Thus, neuronal PrP^C seems to be fundamental for the neurotoxic property of PrP even in the PrP^{Sc}-infected conditions, but the detailed molecular events especially with non-mutant, wild-type PrP^C still remained unclear.

Meanwhile, aged transgenic mice harboring a high-copy-number of wild-type PrP-B transgenes spontaneously developed mitochondrial encephalomyopathy including focal vacuolation of the central nervous system, skeletal muscles and peripheral nerves without PrP^{Sc} inoculation [28]. Such focal vacuolation was localized to the hippocampus, the superior colliculus, and midbrain tegmentum, which resembled that seen in experimental scrapie, albeit less intense. Other transgenic lines harboring a high-copy-number of wild-type PrP transgenes also exhibited spontaneous neurological dysfunction in an age-dependent manner [21,27]. For example, transgenic mice overexpressing the wild-type mouse (Mo) PrP-A gene (Tg(MoPrP)4053/FVB) used in this study became symptomatic at around the age of 700 days, although no pathological evidence for prion diseases was evident [27]. Since no PrP^{Sc} has been inoculated in these mice, investigations of these aged transgenic mice overexpressing wild-type PrP^C may lead to the better understanding how PrP^C participate in the neurotoxic property of PrP.

Here we show that the Tg(MoPrP)4053/FVB mice exhibited an aberrant mitochondrial localization of PrP^C accompanied by decreased mitochondrial manganese superoxide dismutase (Mn-SOD) activity, cytochrome *c* release in the cytosol, caspase-3 activation, and DNA fragmentation, concomitant with decreased proteasomal activity in an age-dependent manner.

Tg(MoPrP)4053/FVB and its littermate were kindly provided by Dr. S.B. Prusiner (University of California, San Francisco). Antibodies K3 and K4 against PrP were rabbit polyclonal sera raised against PrP peptides corresponding to residues 76–90 and 96–110 in MoPrP, respectively. Anti-cytochrome *c* and anti-porin antibodies were purchased from BD Biosciences. Anti-Hsc70 antibody was purchased from Stressgen Biotechnologies Corporation. Mitotracker Red CMXRos was purchased from Molecular Probes. Lactacystin, ALLN, and MG132 were purchased from Sigma. The $\Delta\Psi m$ detection kit and APO-BrdU TUNEL assay kit were purchased from Trevigen Inc. and Molecular Probes, respectively. Antibodies were used at 1:1000 (Western blotting) or 1:100 (immunofluorescence microscopy) unless otherwise noted. For immuno-electronmicroscopy, 10 nm golds were purchased from DAKO.

Cells or brains were homogenized with 9 volumes of mitochondrial buffer (220 mM mannitol, 70 mM sucrose, 10 mM Hepes-KOH, pH 7.4, and 0.1 mM EDTA) and centrifuged at 700 × *g* for 5 min at 4 °C, and the supernatant was further centrifuged at 5000 × *g* for 10 min at 4 °C. The supernatant was used as a post-mitochondrial supernatant. The resulted pellet was washed three times with mitochondrial buffer, resuspended in 9 volumes of the same buffer, and then centrifuged at 2000 × *g* for 2 min at 4 °C followed by 5000 × *g* for 8 min at 4 °C. The pellet was resuspended in 9 volumes of the same buffer, and then centrifuged at 5000 × *g* for 10 min at 4 °C. The final pellet was recovered and stored on ice until use (mitochondrial fraction). The post-mitochondrial supernatant was further centrifuged at 100,000 × *g* for 1 h at 4 °C, and the supernatant was used as cytosolic fraction, and the pellet was resuspended in mitochondrial buffer (microsome fraction). Western blots were performed at 5 μg of total protein/lane.

Mitochondrial manganese superoxide dismutase (Mn-SOD) and cytosolic copper/zinc SOD (Cu/Zinc-SOD) activities were measured by the SOD assay kit (Dojindo Molecular Technologies, Inc.), and cytosolic glutathione (GSH) was measured by the Glutathione quantification kit (Dojindo Molecular Technologies, Inc.) according to the manufacturer's instructions. Caspase-3 activity was measured using the PARP Western Blot Kit (WAKO) according to the manufacturer's instructions. DNA fragmentation was measured by the TUNEL assay (ApopTag® Peroxidase *In situ* Apoptosis Detection Kit, CHEMICON International), which was performed according to the manufacturer's instructions before being visualized with an Olympus CX40 (Olympus Optical Co., Ltd.). Sections were counter-stained by 0.5% methyl green (WAKO) in 0.1 M sodium acetate (pH 4.0).

Proteasomal activity assay was performed as previously described [3,9,31].

Tg(MoPrP)4053/FVB harboring a high-copy-number of wild-type PrP-A transgenes at the age of 520 days (TG520) and an age-matched non-transgenic littermate (WT520) showed similar migration rates of PrP^C on poly acrylamide gel electrophoresis and Western blotting using anti-PrP-antibody K4 (Fig. 1A, PK(−)). As increased resistance to protease K digestion is often a feature of PrP^{Sc}, this was examined in TG520 and WT520. No resistance to proteinase K digestion was detected in any of these mice (Fig. 1A, PK(+)). Histological examinations of the TG520 brains including

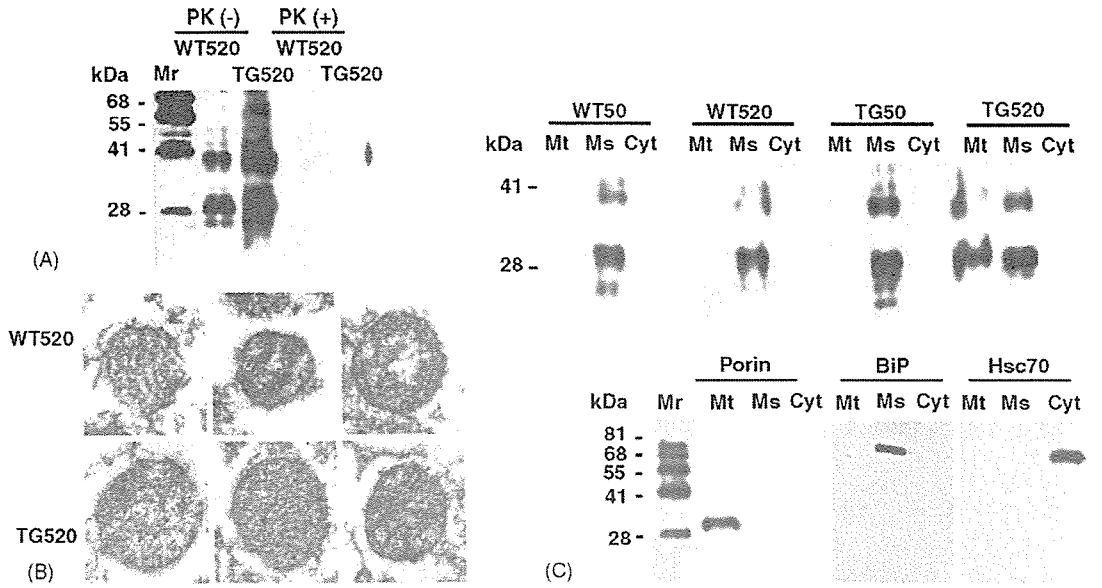

Fig. 1. PrP^C is localized to the mitochondrial fraction in Tg(MoPrP)4053/FVB overexpressing wild-type PrP^C. WT520: non-transgenic littermate at the age of 520 days. TG520: Tg(MoPrP)4053/FVB at the age of 520 days. WT50: non-transgenic littermate at the age of 50 days. TG50: Tg(MoPrP)4053/FVB at the age of 50 days. (A) Western blot analysis and resistance to proteinase K digestion of PrP^C in WT520 and TG520. PK(−): Western blot analysis with anti-PrP antibody K4. Bands derived from PrP^C appear to be normal. PK(+): resistance to proteinase K digestion. Five hundred microliter of brain homogenates (5 μg of total protein/lane) were digested with proteinase K (20 μg/ml, Sigma) at 37 °C for 1 h followed by centrifugation at 100,000 × *g* for 1 h at 4 °C and the resuspended pellet was loaded onto the gels. No resistance to proteinase K digestion is detected. Mr: molecular weight marker. (B) Immuno electron microscopy (30,000×) detects PrP^C with anti-PrP K3 (10 nm golds) in the mitochondria of neuronal cells in TG520. (C) Total brain homogenates of TG520 exhibit aberrant localization of overexpressed PrP^C, whereas those of WT50, WT520 and TG50 do not. Western blot analysis with anti-PrP antibody K4 (1:1000). Anti-porin antibody (1:1000) was used as a mitochondrial (Mt) marker, anti-BiP antibody (1:1000) was used as a microsome (Ms) marker, and anti-Hsc70 antibody (1:1000) was used as a cytosolic (Cyt) marker.

dentate gyrus, hippocampus, other cerebral cortices, basal ganglia and cerebellum by hematoxylin and eosin as well as methyl green-pyronin staining revealed no apparent pathological evidence in the brain sections of WT520 and TG520 (data not shown).

Since older transgenic mice (not inoculated with PrP^{Sc}) that harbor a high-copy-number of wild-type PrP-B transgenes develop mitochondrial encephalomyopathy including focal vacuolation of the central nervous system, skeletal muscles and peripheral nerves [28], we set out to determine whether PrP^C could be detected in the mitochondrial fraction of TG520. Although the TG520 appeared clinically and histologically normal, they exhibited aberrant mitochondrial localization of PrP^C as determined by immuno electron microscopy; immunogold-labelled PrP^C localized at the mitochondria of the granular cells in the hippocampal dentate gyrus of TG520 but not of WT520 (Fig. 1B). Such aberrant mitochondrial localization of PrP^C was further confirmed in TG520 by Western blotting using a subcellular fractionation, whereas younger non-transgenic littermate at the age of 50 days (WT50), WT520, and younger Tg(MoPrP)4053/FVB at the age of 50 days (TG50) did not exhibit the feature (Fig. 1C).

The oxidative stress leads to dysfunctions of the respiratory enzymes and the depletion of ATP followed by a decrease in reduced glutathione (GSH) concentration, which triggers the cycle of oxidative stress, mitochondrial dysfunction, and further antioxidant depletion. Exposure of tissue to oxygen free radicals results in lipid peroxidation, protein oxidation and DNA damage, which is in concert with "apoptosis". In order to prevent such damages, mammalian cells are equipped with both non-enzymatic and enzymatic scavenging systems to eliminate oxygen free radicals, anti oxidant enzymes, i.e., SOD, catalase, and glutathione peroxidase are essential to cells in removing O_2^- and hydrogen peroxide (H_2O_2) from the tissues exposed to oxidative stress. Therefore, we next examined mitochondrial Mn-SOD as well as cytosolic Cu/Zn-SOD activities.

The mitochondrial Mn-SOD activity decreased significantly in TG520 compared to that in WT50, TG50, or WT520 (Fig. 2A), whereas no significant difference in the cytosolic copper/zinc SOD (Cu/Zn-SOD) activity was observed among them (Fig. 2B). Furthermore, cytosolic GSH level was dramatically decreased in TG520 but not in WT50, TG50, or WT520 (Fig. 2C). These results indicated that mitochondria-localized PrP^C induced oxidative stress in TG520.

Subsequently, release of cytochrome *c* from the inner-membrane space into the cytosol (Fig. 3A), caspase-3 activation (Fig. 3B), and DNA fragmentation (Fig. 3C) were observed in TG520 brain, whereas no release of cytochrome *c*/ DNA fragmentation but faint caspase-3 activation was detected in WT520 brain (Fig. 3A–C). Serial specimens of TG520 and WT520 brains were further examined by

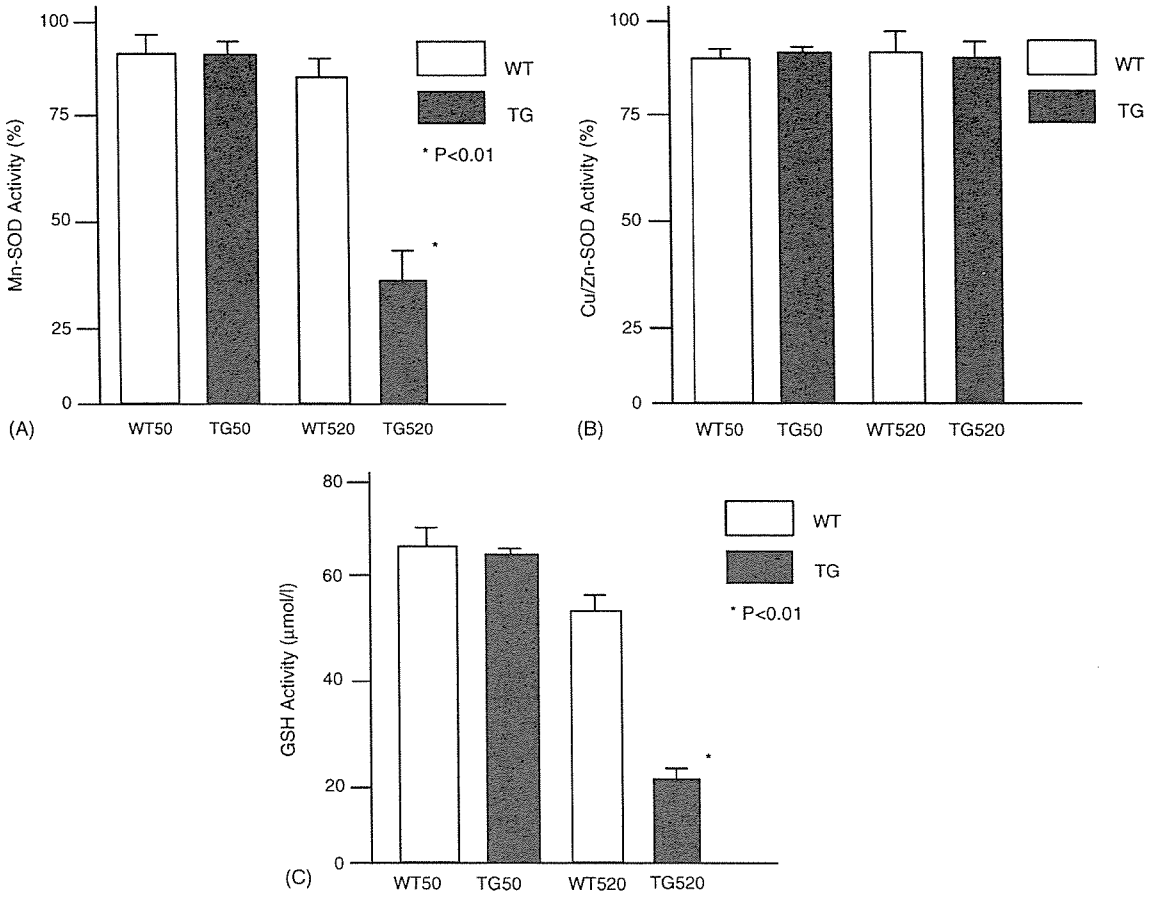

Fig. 2. Mitochondria-localized PrP^C induces oxidative stress in TG520. (A) Mitochondrial manganese superoxide dismutase (Mn-SOD) and (B) cytosolic copper/zinc SOD (Cu/Zinc-SOD) activities. The Mn-SOD activity decreases significantly in TG520 compared to that in WT50, TG50 or WT520, whereas the cytosolic Cu/Zn-SOD activity remained similar among them. Error bars represent mean ± S.D. (C) Cytosolic glutathione (GSH) level is dramatically decreased in TG520 but not in WT50, TG50, or WT520. Error bars represent mean ± S.D.

the TUNEL assay (Fig. 3D). As shown, the TUNEL assay showed that the DNA fragmentation most predominantly in granular cells in the hippocampal dentate gyrus and to a lesser extent pyramidal cells in the CA1 and CA2 regions of TG520 (Fig. 3D).

In an age-dependent development of other aggregation disorders, the accumulation and aggregation of the disease related-proteins are associated with an age-dependent decrease in proteasomal activity and are promoted by inhibition of proteasomal activity [31]. Therefore, it is also likely that such aberrant mitochondrial localization requires PrP^C retained in the cytoplasm with the proteasomal activity decreased. Therefore, the hydrolysis of Suc-Leu-Leu-Val-Tyr-4-methyl-coumaryl-7-amide (Suc-LLVY-MCA) by chymotrypsin-like proteasomal activity in brain homogenates of WT50, WT520, TG50, and TG520 was then investigated. As expected, proteasomal activity of both transgenic mice Tg(MoPrP)4053/FVB and non-transgenic littermate decreased with increasing age (Fig. 3E).

The posttranslational conformational change of PrP^C into PrP^{Sc} is the fundamental process underlying the pathogenesis of prion diseases [24]. Many concurrent reports have suggested that PrP^C may play a role in neuronal survival or death. The removal of serum from cells in culture causes apoptosis in PrP^C-deleted cells but not in wild-type cells [13]. PrP^C also inhibits Bax-mediated neuronal apoptosis in human primary neurons [1]. The binding of a ligand to PrP^C transduces neuroprotective signaling through a cAMP/PKA-dependent pathway. Therefore, PrP^C may function as a trophic receptor whose activation results in a neuroprotective state [5].

On the other hand, misfolded PrP^C is subject to degradation by proteasomes. Like many misfolded secretory proteins [12,23], it is recognized in the ER and subject to retrograde transport to the cytoplasm and degradation by the proteasome [11,14,29,30]. Or, a small fraction of PrP chains is not translocated into the ER lumen during synthesis, and is rapidly degraded in the cytoplasm by the proteasome as far as proteasome function remains normal [8]. As proteasome function gradually decreases with age over a very long period or with inhibitors in the case of cultured cells, PrP^C overflows in the cytoplasm, targeted to the mitochondria, which subsequently induces the mitochondria-mediated apoptosis.

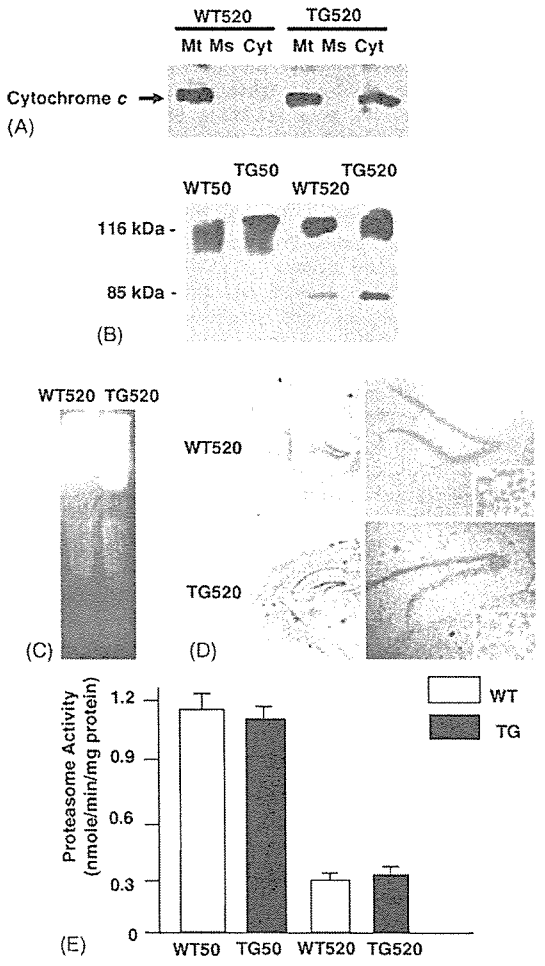

Fig. 3. Neuronal apoptosis in the TG520 brain. (A) Measurement of cytochrome *c* released into the cytosol. Western blot analysis with anti-cytochrome *c* antibody detects cytochrome *c* in the cytosol of the TG520 but not WT520 brain. Mt: mitochondrial fraction, Ms: microsome fraction, Cyt: cytosolic fraction. (B) Caspase-3 activation in TG520 brain. Brain homogenates (5 μg of total protein/lane) of younger WT50 and TG50 do not exhibit caspase-3 activation. Note that a faint band is detected in WT520 brain. The 85 kDa bands corresponding to the degradation products of poly ADP-ribose polymerase (PARP, 116 kDa) is a measure of caspase-3 activity. (C) DNA fragmentation in brain homogenates of TG520 is shown (1 μg of genomic DNA/lane). Brain homogenates of WT520 show no DNA fragmentation. Genomic DNAs were applied onto 1% agarose gel. (D) Serial frozen sections of total brains (left panels) and the hippocampal regions (right panels, 40×, lower right corner panels, 400×) were made. Top panels: WT520. Bottom panels: TG520. Neuronal apoptosis (brown) is evident in the bottom panels as compared with the top panels. (E) Age-dependent decrease in brain proteasomal activity. Chymotrypsin-like proteolytic activity was assayed in brain homogenates (1 μg of total protein/assay) of WT50, TG50, WT520, and TG520. Error bars represent mean ± S.D. ($n = 3$).

In fact, accumulation of PrP^C in the cytoplasm is known to be strongly neurotoxic in both transgenic mice overexpressing the cytosolic form of PrP^C [15] and cyclosporin A-treated cultured cells [7]. In these systems, PrP^C expression enhances staurosporine-stimulated neuronal toxicity and DNA fragmentation, caspase-3-like activity and p53 transcriptional activities, all of which suggests that PrP^C sensitizes neurons to apoptotic stimuli through caspase-3-mediated activation [20]. Proteasome inhibitors increase PrP^C-like immunoreactivity and unmask basal caspase-3 activation [19].

Despite these efforts, little is known about the PrP^C localization and its metabolic fate in the cytoplasm. Ma et al. reported that PrP accumulated in the cytoplasm when proteasomal activity was compromised, and PrP^C formed aggregates, often in association with Hsc70 [14]. With prolonged incubation, these aggregates accumulate in an "aggresome"-like state, surrounding the centrosome. Contrary to this report, other investigators reported there was a prominent shift in the intracellular locations of PrP immunostaining, but there was no "aggresome"-like PrP accumulation in the centrosome region [29]. The PrP signal was especially pronounced around the nucleus, and this signal only partially overlapped with both ER (calnexin, BiP and concanavalin A) and Golgi (wheat germ agglutinin). Thus, further examination has been awaited for determining the precise intracellular localization of PrP^C in the cytoplasmic face.

With an artificial PrP peptide corresponding to PrP residues 106–126 [PrP(106–126)], chronic exposure of primary rat hippocampal cultures to micromolar concentrations of the peptide induces neuronal death with DNA fragmentation in degenerating neurons, having indicated apoptotic cell death [10]. The earliest detectable apoptotic event was the rapid depolarization of mitochondrial membranes, occurring immediately following treatment of cells with PrP(106–126). Subsequently, cytochrome *c* was released and caspase-3 was activated. It has also been demonstrated that the fusogenic peptide PrP(118–135) induced time- and dose-dependent apoptosis in rat cortical and retinal neurons that included caspase-3 activation and DNA condensation/fragmentation [4,22]. These results have implicated mitochondria as the primary site of action [18]. Unfortunately, this implication has been restricted to the cell death with the artificial PrP peptides, and thereby further illustrates the significance of our current observations in terms of the neurotoxic property of wild-type PrP^C in vitro and in vivo.

There are potentially other mechanisms involved in neurotoxicity of the PrP^{Sc}-infected conditions, for example astrocytes, microglial cells and cytokines [17,25]. The activation of glial cells, which precedes neuronal death, and subsequent release of cytokines/chemokines may also contribute directly or indirectly to the neuronal cell death in prion diseases. In mutant PrP^C metabolism, on the other hand, the ER also seems to play another important role as well. Mutant PrP(Q217R) remains associated with the chaperone BiP at the ER for an abnormally long period of time and is degraded by the proteasomal pathway [11]. Nonetheless, our current observations suggest that wild-type PrP^C participate in the prion neurodegenerative cascade through the mitochondria-mediated events, at least in part. At the same time, the segregation of the infectious and neurotoxic properties of PrP suggests a new therapeutic strategy since prevention of mitochondrial mislocalization of PrP^C can be regarded as putative therapeutic targets aimed at protecting

cells from mitochondria-mediated apoptosis, even though the prion infection is not fully preventable.

Acknowledgements

We thank S.B. Prusiner for providing Tg(MoPrP)4053/FVB, T. Onodera for providing HpL3-4 cells, E. Nannri, K. Ishibashi, C. Ota, Y. Yamaura, and S. Wajima for technical assistance. We are indebted to G. Schatz, T. Omura, K. Mihara, R. Scheckman, and T. Momoi for helpful comments. This work was supported by grants from the Core Research for Evolutional Science and Technology (CREST) of the Japan Science and Technology Agency, Health and Labour Sciences Research Grants, Research on Advanced Medical Technology, nano-001, and the Ministry of Health, Labor and Welfare of Japan.

References

[1] Y. Bounhar, Y. Zhang, C.G. Goodyer, A. LeBlanc, Prion protein protects human neurons against Bax-mediated apoptosis, J. Biol. Chem. 276 (2001) 39145–39149.
[2] S. Brandner, S. Isenmann, A. Raeber, M. Fischer, A. Sailer, Y. Kobayashi, S. Marino, C. Weissmann, A. Aguzzi, Normal host prion protein necessary for scrapie-induced neurotoxicity, Nature 379 (1996) 339–343.
[3] N. Canu, C. Barbato, M.T. Ciotti, A. Serafino, L. Dus, P. Calissano, Proteasome involvement and accumulation of ubiquitinated proteins in cerebellar granule neurons undergoing apoptosis, J. Neurosci. 20 (2000) 589–599.
[4] J. Chabry, C. Ratsimanohatra, I. Sponne, P.P. Elena, J.P. Vincent, T. Pillot, In vivo and in vitro neurotoxicity of the human prion protein (PrP) fragment P118–135 independently of PrP expression, J. Neurosci. 23 (2003) 462–469.
[5] L.B. Chiarini, A.R. Freitas, S.M. Zanata, R.R. Brentani, V.R. Martins, R. Linden, Cellular prion protein transduces neuroprotective signals, EMBO J. 21 (2002) 3317–3326.
[6] R. Chiesa, D.A. Harris, Prion diseases: what is the neurotoxic molecule? Neurobiol. Dis. 8 (2001) 743–763.
[7] E. Cohen, A. Taraboulos, Scrapie-like prion protein accumulates in aggresomes of cyclosporin A-treated cells, EMBO J. 22 (2003) 404–417.
[8] B. Drisaldi, R.S. Stewart, C. Adles, L.R. Stewart, E. Quaglio, E. Biasini, L. Fioriti, R. Chiesa, D.A. Harris, Mutant PrP is delayed in its exit from the endoplasmic reticulum, but neither wild-type nor mutant PrP undergoes retrotranslocation prior to proteasomal degradation, J. Biol. Chem. 278 (2003) 21732–21743.
[9] M.E. Figueiredo-Pereira, K.A. Berg, S. Wilk, A new inhibitor of the chymotrypsin-like activity of the multicatalytic proteinase complex (20S proteasome) induces accumulation of ubiquitin-protein conjugates in a neuronal cell, J. Neurochem. 63 (1994) 1578–1581.
[10] G. Forloni, N. Angeretti, R. Chiesa, E. Monzani, M. Salmona, O. Bugiani, F. Tagliavini, Neurotoxicity of a prion protein fragment, Nature 362 (1993) 543–546.
[11] T. Jin, Y. Gu, G. Zanusso, M. Sy, A. Kumar, M. Cohen, P. Gambetti, N. Singh, The chaperone protein BiP binds to a mutant prion protein and mediates its degradation by the proteasome, J. Biol. Chem. 275 (2000) 38699–38704.
[12] R.R. Kopito, ER quality control: the cytoplasmic connection, Cell 88 (1997) 427–430.
[13] C. Kuwahara, A.M. Takeuchi, T. Nishimura, K. Haraguchi, A. Kubosaki, Y. Matsumoto, K. Saeki, T. Yokoyama, S. Itohara, T. Onodera, Prions prevent neuronal cell-line death, Nature 400 (1999) 225–226.
[14] J. Ma, S. Lindquist, Wild-type and PrP and a mutant associated with prion disease are subject to retrograde transport and proteasome degradation, Proc. Natl. Acad. Sci. U.S.A. 98 (2001) 14955–14960.
[15] J. Ma, R. Wollmann, S. Lindquist, Neurotoxicity and neurodegeneration when PrP accumulates in the cytosol, Science 298 (2002) 1781–1785.
[16] G. Mallucci, A. Dickinson, J. Linehan, P.C. Klohn, S. Brandner, J. Collinge, Depleting neuronal PrP in prion infection prevents disease and reverses spongiosis, Science 302 (2003) 871–874.
[17] M. Marella, J. Chabry, Neurons and astrocytes respond to prion infection by inducing microglia recruitment, J. Neurosci. 24 (2004) 620–627.
[18] C.N. O'Donovan, D. Tobin, T.G. Cotter, Prion protein fragment PrP-(106–126) induces apoptosis via mitochondrial disruption in human neuronal SH-SY5Y cells, J. Biol. Chem. 276 (2001) 43516–43523.
[19] E. Paitel, C. Alves da Costa, D. Vilette, J. Grassi, F. Checler, Overexpression of PrPc triggers caspase 3 activation: potentiation by proteasome inhibitors and blockade by anti-PrP antibodies, J. Neurochem. 83 (2002) 1208–1214.
[20] E. Paitel, R. Fahraeus, F. Checler, Cellular prion protein sensitizes neurons to apoptotic stimuli through Mdm2-regulated and p53-dependent caspase 3-like activation, J. Biol. Chem. 278 (2003) 10061–10066.
[21] V. Perrier, K. Kaneko, J. Safar, J. Vergara, P. Tremblay, S.J. DeArmond, F.E. Cohen, S.B. Prusiner, A.C. Wallace, Dominant-negative inhibition of prion replication in transgenic mice, Proc. Natl. Acad. Sci. U.S.A. 99 (2002) 13079–13084.
[22] T. Pillot, B. Drouet, M. Pincon-Raymond, J. Vandekerckhove, M. Rosseneu, J. Chambaz, A nonfibrillar form of the fusogenic prion protein fragment [118-135] induces apoptotic cell death in rat cortical neurons, J. Neurochem. 75 (2000) 2298–2308.
[23] R.K. Plemper, D.H. Wolf, Retrograde protein translocation: ERADication of secretory proteins in health and disease, Trends Biochem. Sci. 24 (1999) 266–270.
[24] S.B. Prusiner, Prions, Proc. Natl. Acad. Sci. U.S.A. 95 (1998) 13363–13383.
[25] J. Schultz, A. Schwarz, S. Neidhold, M. Burwinkel, C. Riemer, D. Simon, M. Kopf, M. Otto, M. Baier, Role of interleukin-1 in prion disease-associated astrocyte activation, Am. J. Pathol. 165 (2004) 671–678.
[26] L. Solforosi, J.R. Criado, D.B. McGavern, S. Wirz, M. Sanchez-Alavez, S. Sugama, L.A. DeGiorgio, B.T. Volpe, E. Wiseman, G. Abalos, E. Masliah, D. Gilden, M.B. Oldstone, B. Conti, R.A. Williamson, Cross-linking cellular prion protein triggers neuronal apoptosis in vivo, Science 303 (2004) 1514–1516.
[27] G.C. Telling, T. Haga, M. Torchia, P. Tremblay, S.J. DeArmond, S.B. Prusiner, Interactions between wild-type and mutant prion proteins modulate neurodegeneration in transgenic mice, Genes Dev. 10 (1996) 1736–1750.
[28] D. Westaway, J. Cayetano-Canlas, D. Groth, D. Foster, S.-L. Yang, M. Torchia, G.A. Carlson, S.B. Prusiner, Degeneration of skeletal muscle, peripheral nerves, and the central nervous system in transgenic mice overexpressing wild-type prion proteins, Cell 76 (1994) 117–129.
[29] Y. Yedidia, L. Horonchik, S. Tzaban, A. Yanai, A. Taraboulos, Proteasomes and ubiquitin are involved in the turnover of the wild-type prion protein, EMBO J 20 (2001) 5383–5391.
[30] G. Zanusso, R.B. Petersen, T. Jin, Y. Jing, R. Kanoush, S. Ferrari, P. Gambetti, N. Singh, Proteasomal degradation and N-terminal protease resistance of the codon 145 mutant prion protein, J. Biol. Chem. 274 (1999) 23396–23404.
[31] H. Zhou, F. Cao, Z. Wang, Z.X. Yu, H.P. Nguyen, J. Evans, S.H. Li, X.J. Li, Huntingtin forms toxic NH_2-terminal fragment complexes that are promoted by the age-dependent decrease in proteasome activity, J. Cell Biol. 163 (2003) 109–118.

Available online at www.sciencedirect.com
SCIENCE DIRECT®
Biochemical and Biophysical Research Communications 327 (2005) 894–899
BBRC
www.elsevier.com/locate/ybbrc

Prion protein with Y145STOP mutation induces mitochondria-mediated apoptosis and PrP-containing deposits in vitro

Naomi S. Hachiya[a,b], Kota Watanabe[a,b], Makiko Y. Kawabata[a,b], Akiko Jozuka[a,b], Yoshimichi Kozuka[c], Yuji Sakasegawa[a], Kiyotoshi Kaneko[a,b,*]

[a] *Department of Cortical Function Disorders, National Institute of Neuroscience (NIN), National Center of Neurology and Psychiatry (NCNP), Kodaira, Tokyo 187-8502, Japan*
[b] *Core Research for Evolutional Science and Technology (CREST), Japan Science and Technology Corporation, Japan*
[c] *Department of Ultrastructural Research, National Institute of Neuroscience (NIN), National Center of Neurology and Psychiatry (NCNP), Kodaira, Tokyo 187-8502, Japan*

Received 2 December 2004
Available online 29 December 2004

Abstract

A pathogenic truncation of an amber mutation at codon 145 (Y145STOP) in Gerstmann–Straussler–Scheinker disease (GSS) was investigated through the real-time imaging in living cells, by utilizing GFP-PrP constructs. GFP-PrP(1–144) exhibited an aberrant localization to mitochondria in mouse neuroblastoma neuro2a (N2a) and HpL3-4 cells, a hippocampal cell line established from *prnp* gene-ablated mice, whereas full-length GFP-PrP did not. The aberrant mitochondrial localization was also confirmed by Western blot analysis. Since GFP-PrP(1–121), as previously reported, and full-length GFP-PrP do not exhibit such mitochondrial localization, the mitochondrial localization of GFP-PrP(1–144) requires not only PrP residues 121–144 (in human sequence) but also COOH-terminal truncation in the current experimental condition. Subsequently, the GFP-PrP(1–144) induced a change in the mitochondrial innermembrane potential ($\Delta\Psi_m$), release of cytochrome *c* from the intermembrane space into the cytosol, and DNA fragmentation in these cells. Non-fluorescent PrP(1–144) also induced the DNA fragmentation in N2a and HpL3-4 cells after the proteasomal inhibition. These data may provide clues as to the molecular mechanism of the neurotoxic property of Y145STOP mutation. Furthermore, immunoelectron microscopy revealed numerous electron-dense deposits in mitochondria clusters of GFP-PrP(1–144)-transfected N2a cells, whereas no deposit was detected in the cells transfected with full-length GFP-PrP. Co-localization of GFP/PrP-immunogold particles with porin-immunogold particles as a mitochondrial marker was observed in such electron-dense vesicular foci, resembling those found in autophagic vacuoles forming secondary lysosomes. Whether such electron-dense deposits may serve as a seed for the growth of amyloid plaques, a characteristic feature of GSS with Y145STOP, awaits further investigations.

Keywords: Cellular prion protein; Green fluorescent protein; PrP Y145STOP mutation; Mitochondria-mediated apoptosis; PrP-containing deposits

Prion protein (PrP) consists of two isoforms, one is a host-encoded cellular isoform (PrP^C) and the other is an abnormal protease-resistant pathogenic isoform (PrP^{Sc}), of which the latter is a causative agent of prion disease. PrP^{Sc} stimulates the conversion of PrP^C into nascent PrP^{Sc}, and the accumulation of PrP^{Sc} leads to central nervous system dysfunction and neuronal degeneration both in humans and animals [1]. The human prion diseases include kuru, Creutzfeldt–Jakob disease, Gerstmann–Straussler–Scheinker disease (GSS), and fatal familial insomnia [2,3].

* Corresponding author. Fax: +81 42 346 1748.
E-mail address: kaneko@ncnp.go.jp (K. Kaneko).

0006-291X/$ - see front matter © 2004 Elsevier Inc. All rights reserved.
doi:10.1016/j.bbrc.2004.12.079

We previously demonstrated the microtubule-associated intracellular localization of the NH_2-terminal fluorescent PrP^C fragment [4] in mouse neuroblastoma neuro2a (N2a) and HpL3-4 cells, a hippocampal cell line established from *prnp* gene-ablated mice [5], by utilizing double-labeled PrP^C. We detected NH_2-terminally fluorescent-tagged PrP^C predominantly in the intracellular compartments, COOH-terminally fluorescent-tagged PrP^C mostly at the cell surface membranes overlapping with lipid rafts, and PrP^C in full length with the merged color in Golgi compartments. Truncated PrP^C with the amino acid residues 1–121, 1–111, and 1–91 in mouse PrP exhibited a proper distribution profile. Following real-time imaging analysis with GFP-PrP^C revealed that the discrete NH_2-terminal amino acid residues are indispensable for the anterograde and the retrograde intracellular movements of GFP-PrP^C [6]. Consistent with our reports, other groups also found the GFP-tagged version of PrP^C to be properly anchored at the cell surface and its distribution pattern to be similar to that of the endogenous PrP^C, with labeling at the plasma membrane and in an intracellular perinuclear compartment [7–11].

Meanwhile, a pathogenic truncation of an amber mutation at codon 145 (Y145STOP) in the *prnp* gene, which was identified in a Japanese patient with GSS [12], came to our notice. The Y145STOP in human *prnp* gene corresponds to Y144STOP in mouse *prnp* gene which yields a product, mouse PrP(1–143) but hereafter designated PrP(1–144), and results in intracellular accumulation if proteasomal degradation is impaired [13]. Until now, its precise subcellular localization and relevance to the neurotoxic property have not been well characterized. Hence, GFP version of PrP(1–144) transgene was constructed and transfected in two independent cell lines, N2a and HpL3-4 cells.

Here we demonstrate for the first time that GFP-PrP(1–144) exhibited an aberrant mitochondrial localization accompanied by the depolarization of mitochondrial innermembrane, cytochrome *c* release in the cytosol, DNA fragmentation, and the formation of numerous PrP-containing deposits in intracellular vacuoles resembling secondary lysosomes.

Materials and methods

Construction of GFP-PrP and GFP-PrP(1–144). GFP-PrP constructs were made as previously described [4,6], and the resulted plasmid was designated pSPOX-MHM2PrP::GFP. The mutant was amplified by PCR from the pSPOX-MHM2PrP::GFP (for amino acid residues Δ144–230 in mouse PrP) [4,6], digested with *Bam*HI and *Xho*I, and replaced with the *Bam*HI–*Xho*I fragment of pSPOX-MHM2PrP::GFP [14]. Non-fluorescent PrP constructs were made from the pSPOX-MHM2PrP [14]. The resulted plasmid was verified by direct DNA sequencing.

Antibodies and drugs. Antibody K3 against PrP^C was rabbit polyclonal sera raised against N-terminal PrP peptides corresponding to residues 76–90 in mouse PrP. Anti-cytochrome *c* and anti-porin were purchased from BD Biosciences. Anti-Hsc70 and anti-BiP were purchased from Stressgen Biotechnologies. Anti-GFP was purchased from Sigma. Mitotracker Red CMXRos was purchased from Molecular Probes. Lactacystin, ALLN, and MG132 were purchased from Sigma. The mitochondrial innermembrane potential ($\Delta\Psi_m$) detection kit was purchased from Trevigen. DNA fragmentation was measured by TUNEL (APO-BrdU TUNEL assay kit (Molecular Probes)), which was performed according to the manufacturer's instructions before being visualized with a Delta-Vision microscopy system (Applied Precision), and out-of-focus images were removed by interactive deconvolution. Antibodies were used at 1:1000 (Western blotting) or 1:100 (immunoelectron microscopy) unless otherwise noted. For immunoelectron microscopy, 10 and 20 nm golds were purchased from DAKO.

Cell cultures, DNA transfection, and drug treatments. Mouse N2a cells were obtained from American Tissue Culture Collection, and HpL3-4 cells were provided by Dr. T. Onodera (the University of Tokyo). Cells were grown and maintained at 37 °C in MEM supplemented with 10% fetal bovine serum. N2a and HpL3-4 cells were transiently transfected with each construct using a DNA transfection kit (Lipofectamin, Gibco-BRL). Western blot analyses were performed as described [14]. To inhibit proteasomal function, N2a or HpL3-4 cells were treated with 10 μM lactacystin, ALLN, or MG132 for 3.5 h at 37 °C.

Preparation of mitochondrial, microsomal, and cytosolic fractions [15]. Cells were homogenized with 9 volumes of mitochondrial buffer (220 mM mannitol, 70 mM sucrose, 10 mM Hepes–KOH, pH 7.4, and 0.1 mM EDTA) and centrifuged at 700*g* for 5 min at 4 °C, and the supernatant was further centrifuged at 5000*g* for 10 min at 4 °C. The supernatant was used as a post-mitochondrial supernatant. The resulted pellet was washed three times with mitochondrial buffer, resuspended in 9 volumes of the same buffer, and then centrifuged at 2000*g* for 2 min at 4 °C followed by 5000*g* for 8 min at 4 °C. The pellet was resuspended in 9 volumes of the same buffer and then centrifuged at 5000*g* for 10 min at 4 °C. The final pellet was recovered and stored on ice until use (mitochondrial fraction). The post-mitochondrial supernatant was further centrifuged at 100,000*g* for 1 h at 4 °C, and the supernatant was used as cytosolic fraction, and the pellet was resuspended in mitochondrial buffer (microsomal fraction). Western blots were performed at 5 μg total protein/lane.

Real-time imaging. To observe living cells, cells were cultured on glass-bottomed dishes (Matsunami) for 24–48 h after the DNA transfection. To visualize mitochondria, cells were incubated for 10 min at 37 °C with Mitotracker Red CMXRos at desired concentrations. Images of cells were collected with a Delta Vision Microscopy System (Applied Precision) equipped with an Olympus IX70.

Results

The intracellular localization of fluorescent PrP^C was investigated through the real-time imaging in living cells by utilizing GFP-PrP constructs. It was investigated in N2a cells that can be infected with PrP^{Sc} [16] and has been widely used for studies in the PrP^C metabolism, as well as in HpL3-4 cells, a hippocampal cell line established from *prnp* gene-ablated mice [5].

GFP-PrP(1–144) exhibited an aberrant localization to mitochondria, as demonstrated by its colocalization with the mitochondrial-specific molecule, Mitotracker, in N2a cells (Fig. 1A, upper panels) and HpL3-4 cells (Fig. 1A, lower panels), whereas full-length GFP-PrP did not. Previously, we also demonstrated that GFP-

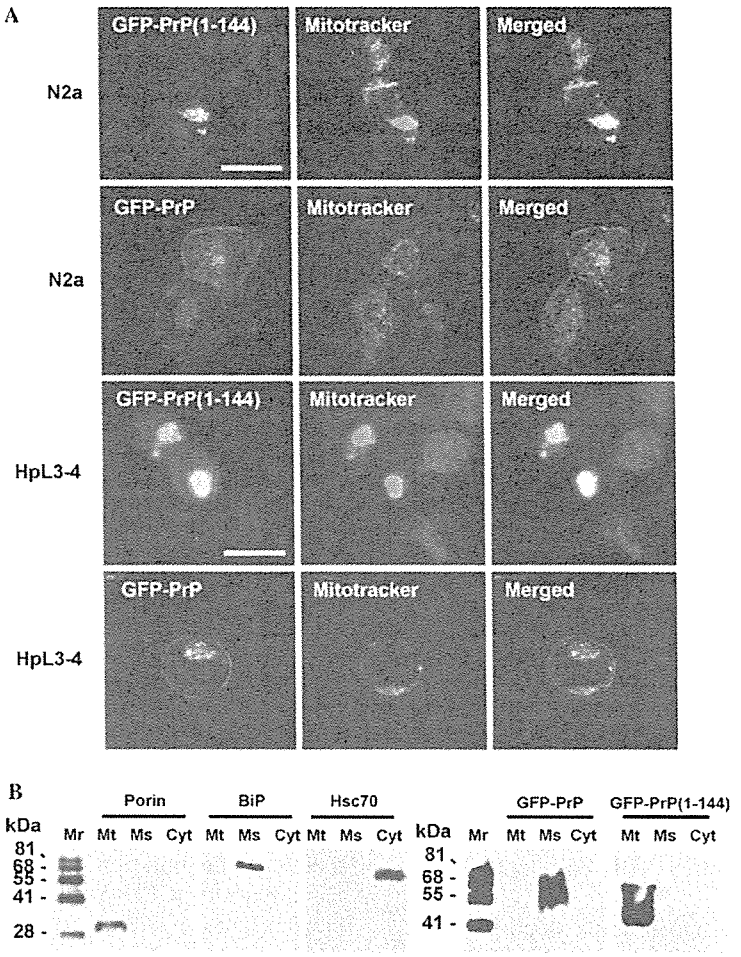

Fig. 1. Mitochondrial localization of GFP-PrP(1–144). GFP-PrP(1–144) exhibits aberrant localization in N2a cells, whereas full-length GFP-PrP does not. (A) GFP-PrP^{C} localization. Full-length GFP-PrP and GFP-PrP(1–144) constructs were made and transfected in N2a (upper panels) and HpL3-4 cells (lower panels). Scale bars = 8 μm. (B) Western blot analysis with anti-GFP antibody. Anti-porin antibody was used as a mitochondrial (Mt) marker, anti-BiP antibody was used as a microsome (Ms) marker, and anti-Hsc70 antibody was used as a cytosolic (Cyt) marker. Mr, molecular weight marker.

PrP(1–121) does not exhibit such mitochondrial localization [4]. Thus, the mitochondrial localization of GFP-PrP(1–144) requires not only PrP residues 121–144 (in human sequence) but also COOH-terminal truncation in the current experimental condition, regardless of whether endogenous full-length PrP^{C} exists. The aberrant mitochondrial localization of GFP-PrP(1–144) was further confirmed by Western blot analysis using a subcellular fractionation method (Fig. 1B).

Subsequently, the GFP-PrP(1–144) induced the depolarization of mitochondrial innermembrane (a change in the $\Delta\Psi_m$) in N2a (Fig. 2A, upper panels) and HpL3-4 cells (Fig. 2A, lower panels), release of cytochrome *c* from the intermembrane space into the cytosol (Fig. 2B), and DNA fragmentation assessed by TUNEL in N2a (Fig. 2C, upper panels) and HpL3-4 cells (data not shown). The PrP(1–144) is normally degraded through the proteasomal pathway, but intracellular accumulation results if proteasomal degradation is impaired [13]. Therefore, we next set out to treat the non-fluorescent PrP(1–144)-transfected cells with proteasome inhibitors including lactacystin, ALLN, or MG132. After the lactacystin treatment, non-fluorescent PrP(1–144) induced the DNA fragmentation in N2a (Fig. 2C, lower panels) and HpL3-4 cells (data not shown). Treatment with ALLN or MG132 also exhibited similar results (data not shown). These observations are characteristic of the mitochondria-mediated apoptotic process. In contrast, none of these abnormalities was observed in N2a and HpL3-4 cells transfected with full-length GFP-PrP construct.

During these investigations, we noticed that GFP-PrP(1–144)-transfected N2a and HpL3-4 cells lost its normal mitochondrial configurations as if congregated predominantly in an intracellular perinuclear region. To further investigate the ultrastructural

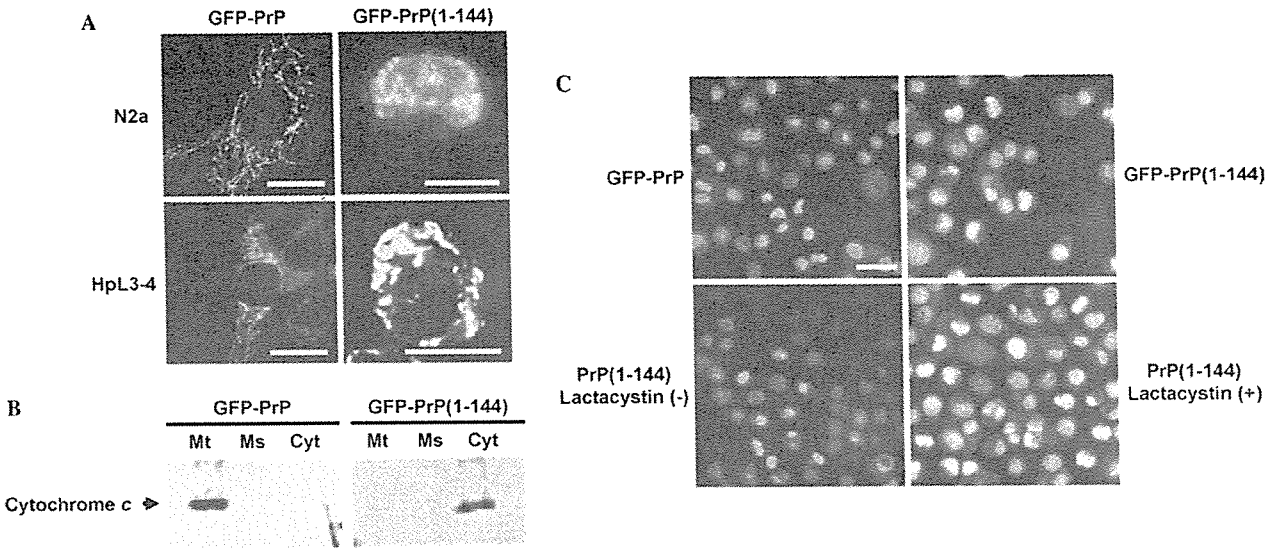

Fig. 2. Accumulation of GFP-PrP(1–144) induces mitochondria-mediated apoptosis. (A) Inactivation of the mitochondrial innermembrane potential ($\Delta\Psi_m$, red; active, green; inactive) in N2a (upper panels) and HpL3-4 (lower panels) cells transfected with GFP-PrP(1–144). Scale bars = 4 μm. (B) The release of cytochrome *c* from the mitochondria in N2a cells transfected with GFP-PrP(1–144). Mt, mitochondria fraction; Ms, microsome fraction; and Cyt, cytosolic fraction. The markers are the same as shown in Fig. 1B. (C) Upper panels: DNA fragmentations measured by TUNEL (red; negative, green; positive) are shown in N2a cells transfected with GFP-PrP(1–144). Lower panels: non-fluorescent PrP(1–144) transfected in N2a cells also exhibits the DNA fragmentation in a lactacystin-dependent manner. Scale bars = 15 μm.

morphology of these mitochondria, we next performed electron microscopy in N2a cells transfected with GFP-PrP(1–144) in comparison with full-length GFP-PrP.

As results, numerous electron-dense deposits were observed in mitochondrial clusters of the GFP-PrP(1–144)-transfected N2a cells, whereas none was detected in N2a cells transfected with full-length GFP-PrP (Fig. 3A). Some vesicles contained myelin-like figures resembling those found in autophagic vacuoles forming secondary lysosomes (Fig. 3B). Co-localization of PrP-immunogolds (Fig. 3C, left panel)/GFP-immunogolds (Fig. 3C, middle panel) with porin-immunogold particles as a mitochondrial marker (Fig. 3C, right panel) was observed in such electron-dense vesicular foci. Non-fluorescent PrP(1–144) also induced the same deposits after the proteasomal inhibition (data not shown).

Discussion

The Y145STOP mutation at PrP residue 145 results in a heritable human prion disease, GSS-like disorder, with extensive PrP amyloid deposits in cerebral parenchyma and vessels [12,17]. The Y145STOP, which yields a product of PrP(1–144), lacks GPI-anchor and is normally degraded through the proteasomal pathway, and also results in intracellular accumulation if proteasomal degradation is impaired [13]. Most PrP(1–144) is degraded very rapidly by the proteasome-mediated pathway, and thus blockage of proteasomal degradation results in intracellular accumulation of PrP(1–144). From the current results, however, the GFP-tagged PrP(1–144) seems to be more metabolically stable, and therefore GFP-PrP(1–144) expression itself is sufficient to induce its intracellular accumulation. In fact, non-fluorescent PrP(1–144) required the treatment with proteasome inhibitors to exhibit the same features.

In this paper, we revealed for the first time the site of intracellular accumulation and the neurotoxic property of mutant PrP^C, Y145STOP, in a human GSS model. The GFP-PrP(1–144) exhibited an aberrant localization to mitochondria, and subsequent mitochondria-mediated apoptosis was induced. Misfolded PrP^C is subjected to degradation by proteasomes, and accumulation of PrP^C in the cytosol is strongly neurotoxic in transgenic mice [18] and cyclosporin A-treated cultured cells [19], and proteasome inhibitors increase PrP^C-like immunoreactivity and unmasked a basal caspase 3 activation [20]. Concomitant with decreased proteasomal activity, aberrant mitochondrial localization of PrP^C followed by mitochondria-mediated neuronal apoptosis was also detected in aged transgenic mice overexpressing wild-type mouse PrP^C, but only after 520 days after birth [15]. These mice develop a spontaneous neurological dysfunction in an age-dependent manner [21,22]. Taken together, a PrP^C load in the cytosol induces the mitochondrial localization of PrP^C with subsequent mito-